Published for SISSA by Springer

Received: *September 26, 2023*
Revised: *November 21, 2023*
Accepted: *January 15, 2024*
Published: *January 30, 2024*

Measurement of the $e^+e^- \to K^0_S K^0_L \pi^0$ cross sections from $\sqrt{s} = 2.000$ to 3.080 GeV

The BESIII collaboration

E-mail: besiii-publications@ihep.ac.cn

Abstract: Based on e^+e^- collision data collected at center-of-mass energies from 2.000 to 3.080 GeV by the BESIII detector at the BEPCII collider, a partial wave analysis is performed for the process $e^+e^- \to K^0_S K^0_L \pi^0$. The results allow the Born cross sections of the process $e^+e^- \to K^0_S K^0_L \pi^0$, as well as its subprocesses $e^+e^- \to K^*(892)^0 \bar{K}^0$ and $K^*_2(1430)^0 \bar{K}^0$ to be measured. The Born cross sections for $e^+e^- \to K^0_S K^0_L \pi^0$ are consistent with previous measurements by BaBar, but with substantially improved precision. The Born cross section lineshape of the process $e^+e^- \to K^*(892)^0 \bar{K}^0$ is consistent with a vector meson state around 2.2 GeV with a significance of 3.2σ. A Breit-Wigner fit determines its mass as $M_Y = (2164.7 \pm 9.1 \pm 3.1)\,\mathrm{MeV}/c^2$ and its width as $\Gamma_Y = (32.4 \pm 21.0 \pm 1.8)\,\mathrm{MeV}$.

Keywords: e^+-e^- Experiments, Particle and Resonance Production, Spectroscopy

ArXiv ePrint: 2309.13883

https://doi.org/10.1007/JHEP01(2024)180

Contents

1 Introduction

The vector meson state $Y(2175)$, denoted as $\phi(2170)$ by the Particle Data Group [1], is one of the more interesting particles in the field of light-flavored hadron spectroscopy. It was first observed by the BaBar collaboration [2] and subsequently investigated by the Belle, BES and BESIII collaborations [3–13]. Several interpretations have been proposed for the $\phi(2170)$ state, such as a conventional 3^3S_1 or 2^3D_1 $s\bar{s}$ state [14–17], a $s\bar{s}g$ hybrid [18, 19], a tetraquark state [20–23], a $\Lambda\bar{\Lambda}(^3S_1)$ bound state [24–26], and a $\phi K\bar{K}$ resonance state [27].

Studies of the $\phi(2170)$ have been carried out using various final states such as $\phi\eta$ [7, 28], $\phi\eta'$ [8], $\phi f_0(980)$ [2–6, 9, 29], K^+K^- [10, 30, 31], $K^0_SK^0_L$ [11, 32], $K^*(892)^+K^-$ [12], $K^*_2(1430)^+K^-$ [12], $K^*(892)^+K^*(892)^-$ [13] and other charged excited $K\bar{K}$ states [13]. None of these final states is dominant, and the product of the e^+e^- partial width and the branching fraction (BF) of each final state is consistently below 100 eV. The partial decay width $\Gamma(\phi\eta)$ [7, 28] is less than $\Gamma(\phi\eta')$ [8], which disfavors the hybrid interpretation [18, 19]. This result can be explained by the hadronic transition of a strangeonium-like meson along with $\eta-\eta'$ mixing [33]. The partial width of $K^*(892)^+K^*(892)^-$ is significantly greater than that of $K_1(1400)^+K^-$, as predicted for the 2^3D_1 or 3^3S_1 state [14–17]. However, the BESIII collaboration has observed a clear structure in the cross section line shape of $K_1(1400)^+K^-$ around 2.2 GeV [13], but no enhancement in the cross section line shape for $K^*(892)^+K^*(892)^-$ [13], which disfavors the 2^3D_1 or 3^3S_1 prediction. The BESIII collaboration has also measured a larger partial width of $K^*_2(1430)^+K^-$ compared to $K^*(892)^+K^-$ at center-of-mass (c.m.) energies ($\sqrt{s}$) from 2.000 to 3.080 GeV [12], which contradicts the prediction that the $\phi(2170)$ is the 2^3D_1 strangeonium state [16]. More precise measurements of the decay properties of the $\phi(2170)$ are desirable to better understand the nature of the $\phi(2170)$.

JHEP01(2024)180

The $e^+e^- \to K^0_S K^0_L \pi^0$ [34] and $e^+e^- \to K^0_S K^\pm \pi^\mp$ [28] processes have been investigated by the BaBar collaboration using the initial state radiation (ISR) technique. A Dalitz amplitude analysis was performed for $e^+e^- \to K^0_S K^\pm \pi^\mp$, leading to the determination of the isoscalar and isovector cross sections for $K^*(892)\bar{K}$. A distinct asymmetry between neutral and charged channels is observed in the Dalitz plot for $K^0_S\pi^\mp$ and $K^\pm\pi^\mp$ within $\sqrt{s'} = 2$–$3\,\text{GeV}$. It may be related to a similar effect observed in the radiative decay rates of the neutral and charged $K^*_2(1430)$ [28]. The SND collaboration has studied $e^+e^- \to K^0_S K^0_L \pi^0$ at $\sqrt{s} = 1.3 - 2.0\,\text{GeV}$, and the cross sections have been measured at a statistical uncertainty level of 10%-30% [35].

In this paper, we present a partial wave analysis (PWA) of the process $e^+e^- \to K^0_S K^0_L \pi^0$ based on 19 data samples collected by the BESIII experiment, ranging from $\sqrt{s} = 2.000$ to $3.080\,\text{GeV}$ and corresponding to an integrated luminosity of 647 pb^{-1} [36, 37]. The Born cross section of the process $e^+e^- \to K^0_S K^0_L \pi^0$ and its sub-processes $e^+e^- \to K^*(892)^0\bar{K}^0$ and $K^*_2(1430)^0\bar{K}^0$ are measured. Throughout the paper charge conjugated processes are also included by default.

2 BESIII detector and Monte Carlo simulation

The BESIII detector [38] records symmetric e^+e^- collisions provided by the BEPCII storage ring [39], which operates with a peak luminosity of $1\times10^{33}\ \text{cm}^{-2}\text{s}^{-1}$ in the range of $\sqrt{s}$ from 2.0 to 4.95 GeV. BESIII has collected large data samples in this energy region [40]. The cylindrical core of the BESIII detector covers 93% of the full solid angle and consists of a helium-based multilayer drift chamber (MDC), a plastic scintillator time-of-flight system (TOF), and a CsI(Tl) electromagnetic calorimeter (EMC), which are all enclosed in a superconducting solenoidal magnet providing a 1.0 T (0.9 T in 2012) magnetic field. The solenoid is supported by an octagonal flux-return yoke with resistive plate counter muon identification modules interleaved with steel. The charged-particle momentum resolution at $1\,\text{GeV}/c$ is 0.5%, and the $\text{d}E/\text{d}x$ resolution is 6% for electrons from Bhabha scattering. The EMC measures photon energies with a resolution of 2.5% (5%) at 1 GeV in the barrel (end cap) region. The time resolution in the TOF barrel region is 68 ps, while that in the end cap region is 110 ps.

Simulated samples produced with GEANT4 based [41] Monte Carlo (MC) software, which includes the geometric description [42] of the BESIII detector and the detector response, are used to optimize the event selection criteria, estimate backgrounds, and determine the detection efficiency. The signal MC samples for the processes $e^+e^- \to K^0_S K^0_L \pi^0$, $K^*(892)^0\bar{K}^0$ and $K^*_2(1430)^0\bar{K}^0$ are generated by ConExc [43] using an amplitude model with parameters fixed to the PWA results. For background studies, inclusive hadronic events are generated with a hybrid generator that includes ConExc, LUARLW [44] and PHOKHARA [45].

3 Event selection and background analysis

The signal process $e^+e^- \to K^0_S K^0_L \pi^0$ is reconstructed with $K^0_S \to \pi^+\pi^-$, $\pi^0 \to \gamma\gamma$, and K^0_L treated as a missing particle. Signal candidates are required to have two charged pions with zero net charge and at least two photons.

JHEP01(2024)180

Charged tracks detected in the MDC are required to be within a polar angle (θ) range of $|\cos\theta| < 0.93$. Here, θ is defined with respect to the z-axis, which is the symmetry axis of the MDC. Each K^0_S candidate is reconstructed from two oppositely charged tracks satisfying that the distance of closest approach to the interaction point (IP) must be less than 20 cm along the z-axis. The two charged tracks are assigned as $\pi^+\pi^-$ without imposing further particle identification criteria. They are constrained to originate from a common vertex and are required to have an invariant mass within $|M(\pi^+\pi^-) - m_{K^0_S}| < 12\,\mathrm{MeV}/c^2$, where $M(\pi^+\pi^-)$ is the invariant mass of $\pi^+\pi^-$ pair with kinematics updated by the vertex fit and $m_{K^0_S}$ is the K^0_S nominal mass [1]. The decay length of the K^0_S candidate is required to be greater than twice the vertex resolution away from the IP.

Photon candidates are identified using showers in the EMC. The deposited energy of each shower must be more than 25 MeV in the barrel region ($|\cos\theta| < 0.80$) and more than 50 MeV in the end cap region ($0.86 < |\cos\theta| < 0.92$). To exclude showers that originate from charged tracks, the angle subtended by the EMC shower and the position of the closest charged track at the EMC must be greater than 10° as measured from the IP. To suppress electronic noise and showers unrelated to the event, the difference between the event start time and the EMC time of the photon candidate is required to be within [0, 700] ns.

To suppress background and improve the kinematic resolution, a one-constraint (1C) kinematic fit imposing energy-momentum conservation is carried out under the $K^0_S K^0_L\gamma\gamma$ hypothesis with K^0_L treated as a missing particle. If there are more than two photons in an event, the combination with the minimum $\chi^2_{\rm 1C}$ is retained for further analysis, and candidate events are required to satisfy $\chi^2_{\rm 1C} < 30$. To suppress the contamination from the process $e^+e^- \to \gamma_{\rm ISR}K^0_S K^0_L$, an additional 1C kinematic fit is performed under the hypothesis of $\gamma K^0_S K^0_L$, and only events which satisfy $\chi^2_{\rm 1C} < \chi^2_{\rm 1C}(\gamma K^0_S K^0_L)$ are retained. To remove K^0_L showers in the EMC that could be mistaken as photons, the angles between the candidate EMC shower and the K^0_L momentum after the kinematic fit are required to be greater than 20°. Each signal candidate is required to have the invariant mass of the two photons within the π^0 mass region ($|M(\gamma\gamma) - m_{\pi^0}| < 0.015\,\mathrm{GeV}/c^2$).

Potential background sources are studied by analyzing inclusive $e^+e^- \to$ hadrons and exclusive $e^+e^- \to \pi^+\pi^-\pi^0\pi^0$, $K^0_S K^\pm\pi^\mp\pi^0$ and $K^0_S K^0_L\pi^0\pi^0$ MC samples after applying the same event selection criteria. The dominant background process is $e^+e^- \to \pi^+\pi^-\pi^0\pi^0$. Exclusive $e^+e^- \to \pi^+\pi^-\pi^0\pi^0$ events are generated by PHOKHARA [45] based on the results of the BaBar collaboration [46]. The $e^+e^- \to K^0_S K^\pm\pi^\mp\pi^0$ and $e^+e^- \to K^0_S K^0_L\pi^0\pi^0$ events are generated by ConExc based on the dressed cross sections for $e^+e^- \to K^0_S K^\pm\pi^\mp\pi^0$ and $e^+e^- \to K^0_S K^0_L\pi^0\pi^0$ from the BaBar experiment [34, 47] with a phase space model and re-weighted to improve the agreement with BESIII data using a multidimensional gradient-boosting algorithm (HEPML) [48], respectively. The exclusive $e^+e^- \to \pi^+\pi^-\pi^0\pi^0, K^0_S K^\pm\pi^\mp\pi^0$ and $K^0_S K^0_L\pi^0\pi^0$ samples, which have been normalized to the experimental integrated luminosity, are used to evaluate the numbers of background events. The contribution of K^0_S peaking background events from $e^+e^- \to K^0_S K^\pm\pi^\mp\pi^0$ and $K^0_S K^0_L\pi^0\pi^0$ is at a level of $0.1\% - 0.4\%$ for different energy points, which is negligible in the following fit. The background levels are summarized in table 1. Figure 1 shows distributions of the invariant masses of $\pi^+\pi^-$, $M(\pi^+\pi^-)$ and $\gamma\gamma$, $M(\gamma\gamma)$ without the K^0_S and π^0 mass window requirements, respectively.

JHEP01(2024)180

$\sqrt{s}$ (GeV)	Background level	Peaking level
2.0000	5.4%	0.1%
2.0500	5.2%	0.1%
2.1000	6.9%	0.1%
2.1250	6.8%	0.1%
2.1500	6.4%	0.1%
2.1750	5.8%	0.1%
2.2000	6.1%	0.1%
2.2324	6.3%	0.1%
2.3094	6.9%	0.1%
2.3864	6.9%	0.1%
2.3960	7.1%	0.2%
2.6444	8.1%	0.2%
2.6464	8.4%	0.4%
2.9000	8.1%	0.4%
2.9500	9.4%	0.4%
2.9810	8.7%	0.2%
3.0000	7.2%	0.3%
3.0200	8.3%	0.2%
3.0800	8.4%	0.2%

Table 1. Summary of the background level for each $\sqrt{s}$.

Non-K_S^0 events are characterized by a flat shape in $M(\pi^+\pi^-)$ and are estimated with the events in the K_S^0 sideband, which is defined by $0.022 < |M(\pi^+\pi^-) - m_{K_S^0}| < 0.035$ GeV/c^2.

The signal yields of the $e^+e^- \to K_S^0 K_L^0 \pi^0$ process are obtained by performing an unbinned maximum likelihood fit to the $M(\pi^+\pi^-)$ spectrum. The signal component is described by the signal MC-simulated shape convolved with a Gaussian function which describes the difference between data and MC simulation. The mean value and width of the Gaussian function are separately floated parameters at different energy points. The background function is parameterized by a first-order polynomial function. The corresponding fit results for data taken at $\sqrt{s} = 2.125$ and 2.900 GeV are shown in figure 2. The same event selection criteria and fit procedure are applied for all data samples at the nineteen c.m. energies.

In order to improve the resolution of kinematic variables, the remaining $e^+e^- \to K_S^0 K_L^0 \pi^0$ events are subjected to a three-constraint (3C) kinematic fit, which, in addition to imposing energy and momentum conservation, further constrains the π^0 and K_S^0 masses to their PDG values [1]. After all above criteria, the invariant mass spectra of $K_S^0 K_L^0$, $K_S^0\pi^0$, $K_L^0\pi^0$ and the invariant masses squared of $K_S^0\pi^0$ versus $K_L^0\pi^0$ are shown in figure 3, where the $K^*(892)^0$ structure is clear. For the invariant mass spectra of $K_S^0 K_L^0$, $K_S^0\pi^0$ and $K_L^0\pi^0$, the

JHEP01(2024)180

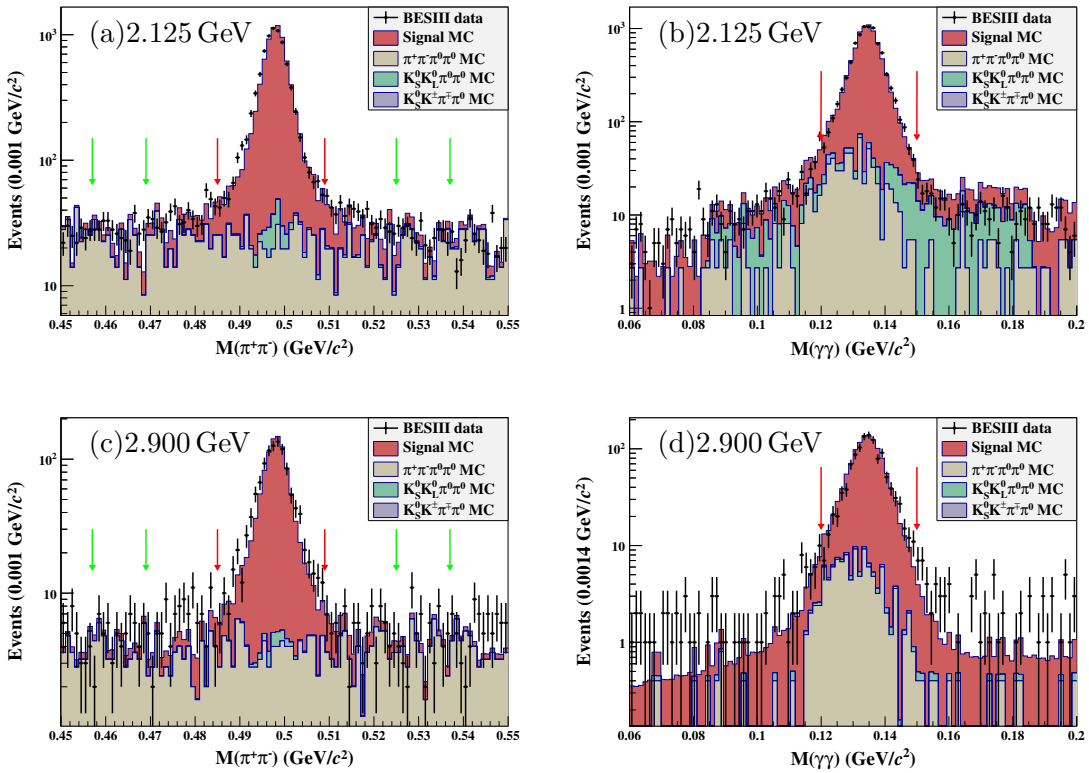

Figure 1. Distributions of (a),(c) $M(\pi^+\pi^-)$ with π^0 mass window requirement and (b),(d) $M(\gamma\gamma)$ at $\sqrt{s} = 2.125$ and 2.900 GeV, where the (black) dots with error bars are data, and the shaded histogram are the stacked MC samples of the signal process, $\pi^+\pi^-\pi^0\pi^0$, $K^0_SK^0_L\pi^0\pi^0$ and $K^0_SK^\pm\pi^\mp\pi^0$. The region between red arrows is the signal region, and the regions between the green arrows are the sideband regions.

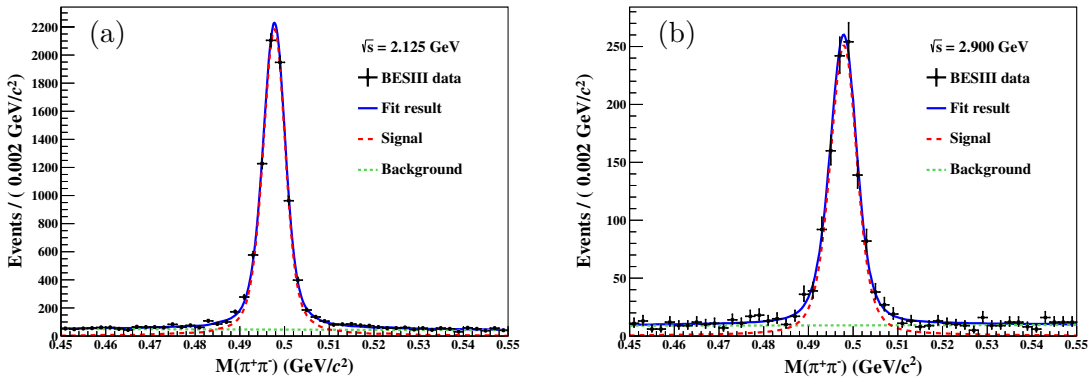

Figure 2. Fit to the $M(\pi^+\pi^-)$ distribution at $\sqrt{s} = 2.125$ and 2.900 GeV, where the black dots with error bars are data, the blue solid curve is the total fit result, the green dashed curve indicates the fitted background shape, and the red dashed curve is the fitted signal shape.

JHEP01(2024)180

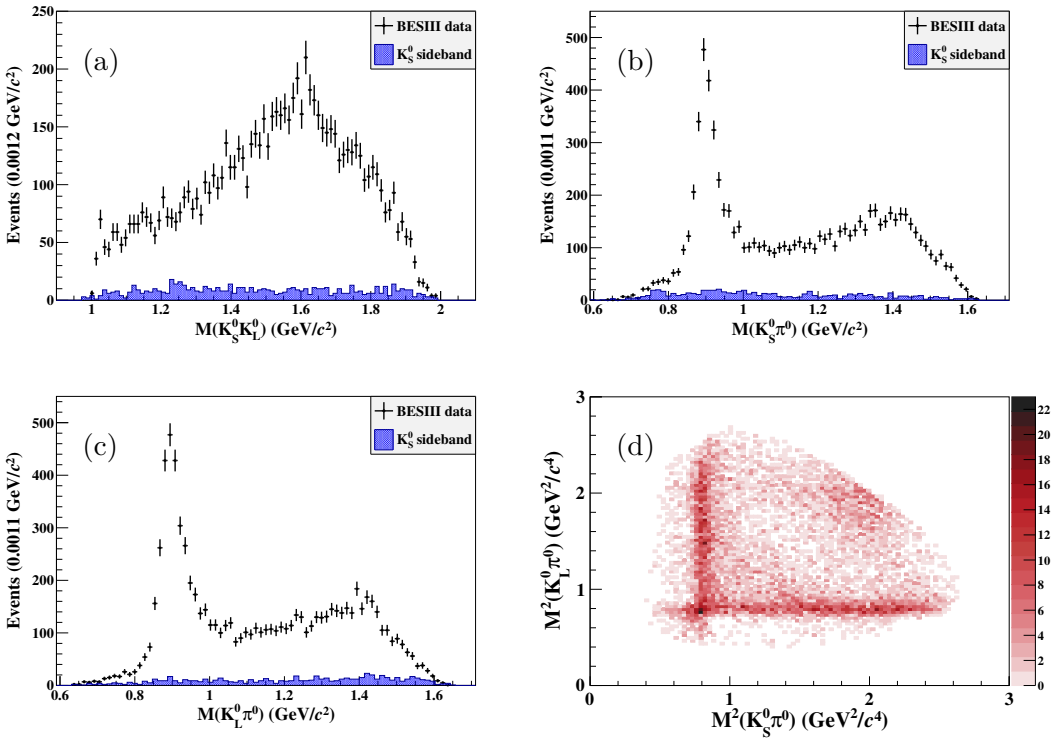

Figure 3. Distributions of (a) $M(K_S^0K_L^0)$, (b) $M(K_S^0\pi^0)$ and (c) $M(K_L^0\pi^0)$, where the (black) dots with error bars are data, and the shaded histograms are non-K_S^0 events estimated by the K_S^0 sideband. (b) Distribution of $M^2(K_S^0\pi^0)$ versus $M^2(K_L^0\pi^0)$. All plots are based on data at $\sqrt{s} = 2.125\,\text{GeV}$.

contributions of background events which are obtained by the K_S^0 sideband are smooth and confirm that there is no peaking structure. Those non-K_S^0 events are used to estimate the background contributions and those K_S^0 peaking backgrounds are negligible in the following amplitude analysis.

4 Amplitude analysis

Based on the GPUPWA framework [49], a PWA is performed on the surviving candidate events to identify the intermediate processes present in $e^+e^- \to K_S^0K_L^0\pi^0$. The quasi-two-body decay amplitudes in the process $e^+e^- \to K_S^0K_L^0\pi^0$ with two sequential decays $e^+e^- \to R_1\pi^0 \to K_S^0K_L^0\pi^0$ and $e^+e^- \to K_S^0(K_L^0)R_2 \to K_S^0K_L^0\pi^0$ are considered and constructed using the covariant tensor amplitude formalism [50], where R_1 and R_2 are the intermediate states that can decay to $K_S^0K_L^0$ and $K_S^0(K_L^0)\pi^0$, respectively.

According to ref. [50], the general form for the decay amplitude of a 1^- state (Y) is

$$A(m) = Y_\mu(m)A^\mu = Y_\mu(m)\sum_i \Lambda_i U_i^\mu, \tag{4.1}$$

where $Y_\mu(m)$ is the polarization vector of Y, m is the spin projection of Y, and U_i^μ is the i-th partial-wave amplitude with coupling strength determined by a complex parameter Λ_i. The amplitude U_i^μ is constructed with the spin factor, Blatt-Weisskopf barrier factors

JHEP01(2024)180

and propagators of resonances under the assumption of isobar model [50]. The differential cross-section can be written as

$$\frac{d\sigma}{d\Phi_n} = \frac{1}{2}\sum_m A^\mu A^{*\mu} = \frac{1}{2}\sum_{i,j}\Lambda_i\Lambda_j^*\sum_m U_i^\mu U_j^{*\mu}. \tag{4.2}$$

The spin factor is constructed with the covariant Zemach (Rarita-Schwinger) tensor formalism [50–53] by combining pure-orbital-angular-momentum covariant tensors $\tilde{t}^{(L)}_{\mu_1\ldots\mu_L}$ and the momenta of parent particles together with Minkowski metric $g_{\mu\nu}$ and Levi-Civita symbol $\epsilon_{\mu\nu\lambda\sigma}$. For a process $a \to bc$, the covariant tensors $\tilde{t}^{(L)}_{\mu_1\ldots\mu_L}$ for the final states of pure orbital angular momentum L are

$$\tilde{t}^{(L)}_{\mu_1\ldots\mu_L} = (-1)^L P^{(L)}_{\mu_1\ldots\mu_L\mu_1^{'}\ldots\mu_L^{'}}(p_a) r^{\mu_1^{'}\ldots\mu_L^{'}} B_L(Q_{abc}), \tag{4.3}$$

where $r = p_b - p_c$, $P^{(L)}_{\mu_1\ldots\mu_L\mu_1^{'}\ldots\mu_L^{'}}(p_a)$ is the spin projection operator of the particle a, Q_{abc} is the magnitude of p_b or p_c in the rest system of a. The Blatt-Weisskopf barrier factors $B_L(Q_{abc})$, are derived by assuming a square well interaction potential as

$$B_0(Q_{abc}) = 1, \tag{4.4}$$

$$B_1(Q_{abc}) = \sqrt{\frac{2}{Q_{abc}^2 + Q_0^2}}, \tag{4.5}$$

$$B_2(Q_{abc}) = \sqrt{\frac{13}{Q_{abc}^4 + 3Q_{abc}^2Q_0^2 + 9Q_0^4}}. \tag{4.6}$$

Here $Q^0 = 0.197321/R\,\mathrm{GeV}/c$ is a hadron "scale" parameter, where R is the radius of the centrifugal barrier in fm. In this paper, the radius R is taken to be 0.7 fm.

The propagator of intermediate resonance is parameterized by a relativistic Breit-Wigner (BW) function with an invariant mass dependent width [54]

$$\mathrm{BW}(s) = \frac{1}{m^2 - s - i\sqrt{s}\Gamma(s)}, \tag{4.7}$$

$$\Gamma(s) = \Gamma_0(m^2)\left(\frac{m^2}{s}\right)\left(\frac{p(s)}{p(m^2)}\right)^{2l+1}, \tag{4.8}$$

where s is the invariant mass squared of the daughter particle, m and Γ_0 are the mass and width of the intermediate resonance, respectively, l is the orbital angular momentum for a daughter particle, and $p(s)$ or $p(m^2)$ is the momentum of a daughter particle in the rest frame of the resonance with mass $\sqrt{s}$ or m. To include the resolution effect for the narrow ϕ resonance, the BW function is convolved with a Gaussian function.

The relative magnitudes and phases of the individual intermediate processes are determined by performing an unbinned maximum likelihood fit using MINUIT [55], where the magnitude and phase of the reference amplitude $e^+e^- \to K^*(892)^0\bar{K}^0$ are fixed to 1 and 0, respectively, while those of other amplitudes are free parameters of the fit.

The negative log-likelihood function for observing N events in the data sample is expressed as

$$\mathcal{NLL} = -\sum_i^N \log\frac{\omega_i\epsilon_i}{\int\epsilon\omega d\Phi_3} = -\sum_i^N \log\frac{\omega_i}{\int\epsilon\omega d\Phi_3} + const, \tag{4.9}$$

JHEP01(2024)180

Process	Significance		
	2.125 GeV	2.396 GeV	2.900 GeV
$\phi\pi^0$	13.1σ	8.6σ	9.7σ
$\phi(1680)\pi^0$	11.1σ	12.2σ	8.3σ
$K^*(892)^0\bar{K}^0$	$>30\sigma$	$>30\sigma$	$>30\sigma$
$K_2^*(1430)^0\bar{K}^0$	29.2σ	5.7σ	5.1σ
$K(1680)^0\bar{K}^0$	9.8σ	8.4σ	7.6σ

Table 2. Statistical significances of the intermediate states for data at $\sqrt{s} = 2.125, 2.396$ and 2.900 GeV.

where ω_i is the decay-amplitude squared evaluated from the four-momenta of final particles for the i-th event, ϵ_i is the detection efficiency and Φ is the standard element of phase space. The contribution of background events to the $\mathcal{NLL}$ is canceled out by evaluating the signal model on K_S^0 sideband events injected into the data sample with negative weights.

Conservation of J^{PC} for intermediate states, in the process $e^+e^- \to R_1\pi^0 \to K_S^0K_L^0\pi^0$, allows both $\mathcal{P}$ and $\mathcal{F}$ wave contributions both in $e^+e^- \to R_1\pi^0$ and $R_1 \to K_S^0K_L^0$. In the case of $e^+e^- \to K_S^0(K_L^0)R_2 \to K_S^0K_L^0\pi^0$, the contributions of $\mathcal{P}$, $\mathcal{D}$ and $\mathcal{F}$ waves are all allowed both in the primary and secondary processes. The PWA fit procedure starts by including the $K^*(892)^0\bar{K}^0$ and $K_2^*(1430)^0\bar{K}^0$ as the initial baseline solutions, and then adds one at a time other possible intermediate states which can decay to $K_S^0(K_L^0)\pi^0$ or $K_S^0K_L^0$. The masses and widths of possible intermediate resonances are fixed to their PDG values [1]. Intermediate states are included in the solution if the statistical significance is greater than 5σ, where the statistical significance is evaluated from the changes in likelihood and degrees of freedom with and without the corresponding amplitude included in the PWA fit. The direct decay process without an intermediate resonance is treated as a phase space distribution without a propagator [12]. The procedure is repeated until a best solution is obtained.

The above strategy is implemented individually on the experimental data sets collected at $\sqrt{s} = 2.125, 2.396$ and 2.900 GeV, which have the largest luminosities and yields among the nineteen data sets. As the c.m. energy increases, we test the significance of the process with higher threshold at $\sqrt{s} = 2.900$ GeV, such as $e^+e^- \to K_3^*(1780)^0\bar{K}^0$, which cannot be produced at $\sqrt{s} = 2.125$ GeV. But the significances of these processes are less than 5σ and they are not retained in the final best solution. The statistical significances of the intermediate states and fit fractions for $\sqrt{s} = 2.125$, 2.396 and 2.900 GeV are listed in table 2 and table 3, respectively. For the other sixteen data samples with lower luminosities and limited statistics, the intermediate components are assumed to be the same as those of the nearby c.m. energies with higher statistics. The intermediate component candidates of $\sqrt{s} = 2.000, 2.050, 2.100, 2.150, 2.175, 2.200$, and 2.232 GeV are assumed to be the same as $\sqrt{s} = 2.125$ GeV. The intermediate component candidates of $\sqrt{s} = 2.309, 2.386, 2.644$ and 2.646 GeV are assumed to be the same as $\sqrt{s} = 2.396$ GeV. The remaining datasets are assumed to use the same intermediate components as $\sqrt{s} = 2.900$ GeV. The data for each energy point is fitted individually.

JHEP01(2024)180

Process	Fraction (%)		
	2.125 GeV	2.396 GeV	2.900 GeV
$\phi\pi^0$	0.78±0.56	0.87±0.61	1.82±1.11
$\phi(1680)\pi^0$	2.39±1.23	5.96±2.10	5.22±1.50
$K^*(892)^0\bar{K}^0$	79.89±1.12	86.01±1.38	72.65±2.11
$K_2^*(1430)^0\bar{K}^0$	7.42±0.83	1.93±0.57	1.85±0.82
$K(1680)^0\bar{K}^0$	3.00±1.11	6.73±1.91	5.82±1.96

Table 3. Fit fractions of the intermediate states for data at $\sqrt{s} = 2.125, 2.396$ and 2.900 GeV.

The invariant mass spectra, angular distributions and fit results for $\sqrt{s} = 2.125$ GeV are shown in figure 4.

5 Born cross sections measurement

The Born cross section for $e^+e^- \to K_S^0K_L^0\pi^0$ is obtained at each c.m. energy using

$$\sigma(\sqrt{s}) = \frac{N_{\rm sig}}{\mathcal{L}\cdot\epsilon\cdot(1+\delta)\cdot\frac{1}{|1-\Pi|^2}\cdot\mathcal{B}}, \tag{5.1}$$

where $N_{\rm sig}$ is the number of signal events, $\mathcal{L}$ is the integrated luminosity, ϵ is the efficiency obtained by weighting MC simulation according to the PWA results, $\mathcal{B}$ is the product of BFs in the full decay chain $\mathcal{B} = \mathcal{B}(K_S^0 \to \pi^+\pi^-)\cdot\mathcal{B}(\pi^0 \to \gamma\gamma) = 68.39\%$, which is taken from the PDG [1], $\frac{1}{|1-\Pi|^2}$ is the vacuum polarization (VP) factor [56], and $1+\delta$ is the ISR correction factor, which is obtained by a QED calculation [57]. Both ϵ and $1+\delta$ depend on the line shape of cross sections and are determined by an iterative procedure [11, 58]. The Born cross section for an intermediate process, $e^+e^- \to K^*(892)^0\bar{K}^0$ or $K_2^*(1430)^0\bar{K}^0$, at each energy is obtained with the same approach, where $N_{\rm sig}$ is replaced with the product of the total number of surviving events and the corresponding fraction relative to the total obtained according to the PWA results, and $\mathcal{B}$ is replaced with the product of the BFs of the decays $K_S^0 \to \pi^+\pi^-, \pi^0 \to \gamma\gamma$ and that of the intermediate state ($K^*(892)^0 \to K^0\pi^0 = 33.23\%, K_2^*(1430)^0 \to K^0\pi^0 = 16.60\%$) from the PDG [1], respectively. The Born cross sections are listed in tables 4, 5 and 6, separately for the processes $e^+e^- \to K_S^0K_L^0\pi^0$, $K^*(892)^0\bar{K}^0$ and $K_2^*(1430)^0\bar{K}^0$, respectively.

The previous BESIII measurement [12] with the charged channel $e^+e^- \to K^+K^-\pi^0$ shows that $K_2^*(1430)^+K^-$ is the dominant component, with the fraction of $K^*(892)^+K^-$ at the 2-10% level. However, in this study with the neutral channel $e^+e^- \to K_S^0K_L^0\pi^0$, $K^*(892)^0\bar{K}^0$ is dominant, while $K_2^*(1430)^0\bar{K}^0$ is at the 5% level in the BESIII c.m. energy region. The asymmetry is also observed by BaBar [28] in the production of $K^*(892)^0\bar{K}^0$, $K^*(892)^+K^-$, $K_2^*(1430)^0\bar{K}^0$ and $K_2^*(1430)^+K^-$. To quantify the effect, we define relative ratios of the Born cross sections:

$$\begin{aligned} R(K^*(892)) &= \frac{\sigma(e^+e^- \to K^*(892)^+K^-)}{\sigma(e^+e^- \to K^*(892)^0\bar{K}^0)}, \\ R(K_2^*(1430)) &= \frac{\sigma(e^+e^- \to K_2^*(1430)^+K^-)}{\sigma(e^+e^- \to K_2^*(1430)^0\bar{K}^0)}. \end{aligned} \tag{5.2}$$

JHEP01(2024)180

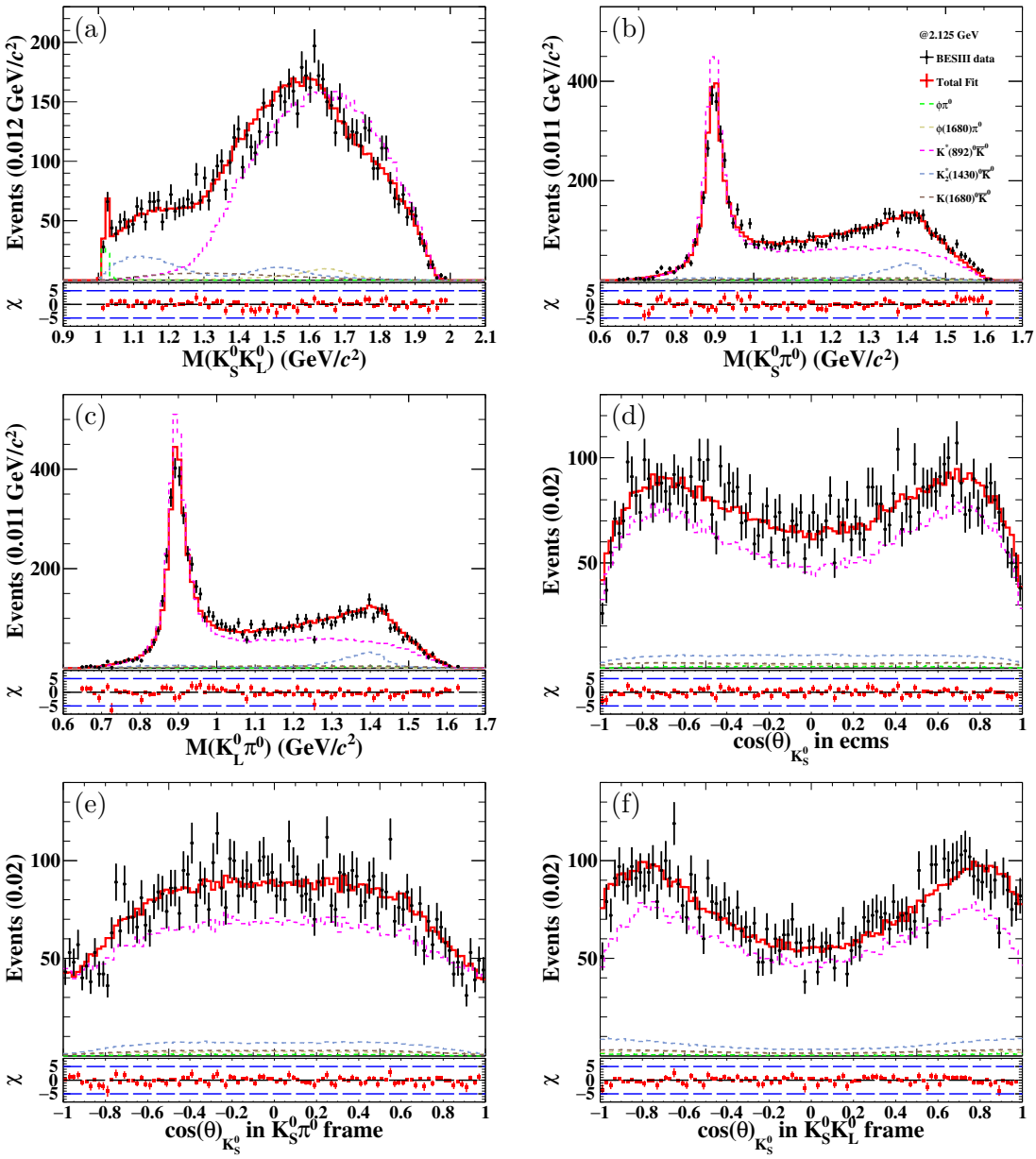

Figure 4. Superposition of data and the PWA fit projections for invariant mass distributions of (a) $K_S^0K_L^0$, (b) $K_S^0\pi^0$ and (c) $K_L^0\pi^0$, and the $\cos\theta$ distributions of (d) K_S^0 in e^+e^- c.m. frame, (e) K_S^0 in $K_S^0\pi^0$ rest frame and (f) K_S^0 in $K_S^0K_L^0$ rest frame at $\sqrt{s} = 2.125\,\text{GeV}$. The pull projection of the residuals is shown beneath each distribution correspondingly. Different styles of the curves denote different components.

JHEP01(2024)180

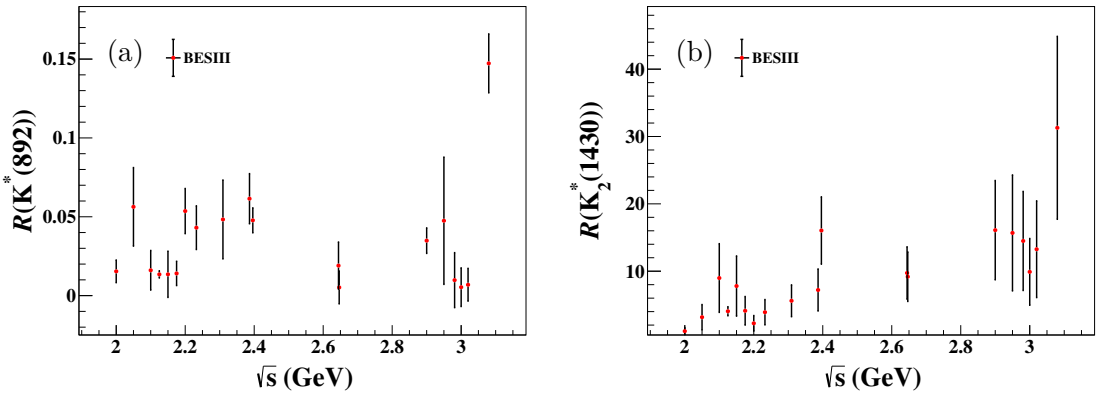

Figure 5. Relative ratio distributions for (a) $K^*(892)$ and (b) $K_2^*(1430)$.

$\sqrt{s}$ (GeV)	$N_{\rm sig}$	$\mathcal{L}$ (pb^{-1})	ϵ	$1+\delta$	$\frac{1}{\lvert 1-\Pi\rvert^2}$	σ (pb)
2.0000	880.6 ± 32.3	10.1 ± 0.1	15.3%	1.22	1.037	$662.7 \pm 24.3 \pm 17.7 \pm 18.0$
2.0500	308.4 ± 19.2	3.34 ± 0.03	15.8%	1.20	1.038	$682.1 \pm 42.5 \pm 18.3 \pm 26.9$
2.1000	941.7 ± 33.8	12.2 ± 0.1	16.4%	1.18	1.039	$557.8 \pm 20.0 \pm 14.9 \pm 15.0$
2.1250	8175.0 ± 98.9	108 ± 1	16.6%	1.17	1.039	$545.4 \pm 6.6 \pm 14.6 \pm 7.2$
2.1500	228.1 ± 16.8	2.84 ± 0.02	17.1%	1.13	1.040	$582.2 \pm 42.9 \pm 15.6 \pm 23.5$
2.1750	678.7 ± 28.4	10.6 ± 0.1	16.5%	1.23	1.040	$444.5 \pm 18.6 \pm 11.9 \pm 16.0$
2.2000	772.8 ± 30.5	13.7 ± 0.1	16.2%	1.25	1.040	$391.2 \pm 15.4 \pm 10.5 \pm 12.2$
2.2324	594.1 ± 26.7	11.9 ± 0.1	16.0%	1.28	1.041	$342.9 \pm 15.4 \pm 9.2 \pm 11.1$
2.3094	846.1 ± 32.8	21.1 ± 0.1	15.5%	1.31	1.041	$277.3 \pm 10.8 \pm 7.4 \pm 10.6$
2.3864	741.3 ± 30.1	22.5 ± 0.2	15.5%	1.34	1.041	$224.2 \pm 9.1 \pm 6.0 \pm 7.9$
2.3960	2146.1 ± 51.2	66.9 ± 0.5	15.2%	1.34	1.041	$220.4 \pm 5.3 \pm 5.9 \pm 4.6$
2.6444	595.2 ± 27.7	33.7 ± 0.2	15.0%	1.45	1.039	$114.4 \pm 5.3 \pm 3.1 \pm 3.2$
2.6464	615.4 ± 27.8	34.0 ± 0.3	15.0%	1.45	1.039	$117.2 \pm 5.3 \pm 3.1 \pm 3.2$
2.9000	1100.7 ± 37.1	105 ± 1	14.0%	1.65	1.033	$64.8 \pm 2.2 \pm 1.7 \pm 1.4$
2.9500	124.0 ± 13.0	15.9 ± 0.1	13.3%	1.68	1.029	$49.6 \pm 5.2 \pm 1.3 \pm 2.3$
2.9810	146.0 ± 13.8	16.1 ± 0.1	13.9%	1.66	1.025	$56.1 \pm 5.3 \pm 1.5 \pm 2.1$
3.0000	144.5 ± 13.9	15.9 ± 0.1	13.7%	1.67	1.021	$56.6 \pm 5.4 \pm 1.5 \pm 2.7$
3.0200	143.8 ± 13.6	17.3 ± 0.1	13.7%	1.71	1.014	$51.1 \pm 4.8 \pm 1.4 \pm 1.9$
3.0800	963.8 ± 35.3	126 ± 1	12.8%	1.83	0.915	$52.3 \pm 1.9 \pm 1.4 \pm 1.2$

Table 4. The measured Born cross sections for $e^+e^- \to K_S^0 K_L^0 \pi^0$, where the first uncertainties are statistical, the second ones are systematics from table 7 and the third ones are model uncertainties.

The corresponding results for the relative ratio are summarized in figure 5.

JHEP01(2024)180

$\sqrt{s}$ (GeV)	$N_{\rm sig}$	$\mathcal{L}$ (pb^{-1})	ϵ	$1+\delta$	$\frac{1}{\lvert 1-\Pi\rvert^2}$	σ (pb)
2.0000	845.4 ± 45.3	10.1 ± 0.1	17.0%	1.07	1.037	$1942.5 \pm 104.0 \pm 52.0 \pm 63.3$
2.0500	225.4 ± 22.8	3.34 ± 0.03	17.2%	1.08	1.038	$1533.4 \pm 155.4 \pm 41.0 \pm 71.1$
2.1000	772.9 ± 52.7	12.2 ± 0.1	17.6%	1.07	1.039	$1420.4 \pm 96.9 \pm 38.0 \pm 46.1$
2.1250	6530.7 ± 120.8	108 ± 1	17.7%	1.05	1.039	$1376.2 \pm 25.5 \pm 36.8 \pm 19.3$
2.1500	200.6 ± 24.4	2.84 ± 0.02	17.1%	1.10	1.040	$1585.8 \pm 193.1 \pm 42.5 \pm 63.0$
2.1750	516.1 ± 31.7	10.6 ± 0.1	17.3%	1.13	1.040	$1055.1 \pm 64.8 \pm 28.2 \pm 33.1$
2.2000	575.5 ± 33.6	13.7 ± 0.1	16.9%	1.14	1.040	$918.5 \pm 53.6 \pm 24.6 \pm 31.0$
2.2324	472.0 ± 26.9	11.9 ± 0.1	16.9%	1.16	1.041	$851.5 \pm 48.5 \pm 22.8 \pm 27.0$
2.3094	637.6 ± 32.5	21.1 ± 0.1	16.4%	1.20	1.041	$648.1 \pm 33.0 \pm 17.3 \pm 22.4$
2.3864	595.6 ± 31.5	22.5 ± 0.2	16.2%	1.23	1.041	$559.5 \pm 29.6 \pm 15.0 \pm 17.3$
2.3960	1845.8 ± 53.0	66.9 ± 0.5	16.4%	1.23	1.041	$578.4 \pm 16.6 \pm 15.5 \pm 11.4$
2.6444	438.0 ± 25.5	33.7 ± 0.2	15.5%	1.35	1.039	$262.0 \pm 15.3 \pm 7.0 \pm 8.1$
2.6464	452.9 ± 25.9	34.0 ± 0.3	15.5%	1.35	1.039	$268.5 \pm 15.3 \pm 7.2 \pm 8.2$
2.9000	799.7 ± 35.6	105 ± 1	14.9%	1.50	1.033	$145.8 \pm 6.5 \pm 3.9 \pm 3.9$
2.9500	94.8 ± 11.0	15.9 ± 0.1	14.3%	1.54	1.029	$115.5 \pm 13.4 \pm 3.1 \pm 6.9$
2.9810	111.6 ± 11.7	16.1 ± 0.1	14.4%	1.56	1.025	$132.0 \pm 13.8 \pm 3.5 \pm 7.3$
3.0000	108.0 ± 11.5	15.9 ± 0.1	14.2%	1.58	1.021	$130.5 \pm 13.9 \pm 3.5 \pm 6.9$
3.0200	104.3 ± 10.8	17.3 ± 0.1	14.2%	1.59	1.014	$115.7 \pm 12.0 \pm 3.1 \pm 6.2$
3.0800	695.9 ± 33.4	126 ± 1	13.3%	1.73	0.915	$115.1 \pm 5.5 \pm 3.1 \pm 2.4$

Table 5. The measured Born cross sections for $e^+e^- \to K^*(892)^0\bar{K}^0$, where the first uncertainties are statistical, the second ones are systematics from table 7 and the third ones are model uncertainties.

6 Systematic uncertainties

Two categories of systematic uncertainties are considered in the measurement of the Born cross sections. The first category includes systematic sources not associated with the PWA fit that are evaluated as follows:

1. The uncertainty associated with the integrated luminosity is 1% and estimated by using large angle Bhabha events [36].

2. The uncertainty concerning K^0_S reconstruction is studied with control samples of $J/\psi \to K^0_S K^\pm \pi^\mp$ and $J/\psi \to \phi K^0_S K^\pm \pi^\mp$. The result shows that the difference in efficiency between data and MC simulation is 1% per K^0_S [59].

3. The uncertainty of the requirement on the number of charged tracks ($N_{\rm charge}$) is estimated with a control sample of $J/\psi \to K^0_S K^0_L \pi^0$. The difference in efficiency between data and MC simulation with and without this requirement is taken as the uncertainty.

4. The uncertainty concerning photon detection efficiency is studied with a control sample of $e^+e^- \to K^+K^-\pi^+\pi^-\pi^0$ [60]. The result shows that the difference in detection efficiency between data and MC simulation is 1% per photon.

JHEP01(2024)180

$\sqrt{s}$ (GeV)	$N_{\rm sig}$	$\mathcal{L}$ (pb^{-1})	ϵ	$1+\delta$	$\frac{1}{\lvert 1-\Pi\rvert^2}$	σ (pb)
2.0000	80.1 ± 28.2	10.1 ± 0.1	20.0%	1.06	1.037	$315.2 \pm 111.2 \pm 8.4 \pm 11.2$
2.0500	11.1 ± 5.0	3.34 ± 0.03	20.4%	1.07	1.038	$127.5 \pm 58.2 \pm 3.4 \pm 6.0$
2.1000	27.3 ± 13.7	12.2 ± 0.1	20.7%	1.07	1.039	$84.6 \pm 42.4 \pm 2.3 \pm 3.6$
2.1250	606.2 ± 68.3	108 ± 1	20.5%	1.08	1.039	$214.2 \pm 24.1 \pm 5.7 \pm 5.2$
2.1500	9.7 ± 5.1	2.84 ± 0.02	23.4%	0.95	1.040	$129.6 \pm 68.1 \pm 3.5 \pm 6.1$
2.1750	59.1 ± 28.6	10.6 ± 0.1	26.1%	0.88	1.040	$204.1 \pm 98.7 \pm 5.5 \pm 7.5$
2.2000	113.1 ± 54.7	13.7 ± 0.1	25.8%	0.96	1.040	$304.0 \pm 147.0 \pm 8.1 \pm 12.2$
2.2324	55.8 ± 25.2	11.9 ± 0.1	23.8%	1.03	1.041	$171.9 \pm 77.8 \pm 4.6 \pm 7.5$
2.3094	54.5 ± 21.6	21.1 ± 0.1	22.3%	1.04	1.041	$94.3 \pm 37.4 \pm 2.5 \pm 4.3$
2.3864	28.0 ± 11.5	22.5 ± 0.2	22.3%	1.07	1.041	$45.3 \pm 18.7 \pm 1.2 \pm 1.8$
2.3960	41.5 ± 12.3	66.9 ± 0.5	21.7%	1.07	1.041	$22.3 \pm 6.6 \pm 0.6 \pm 0.7$
2.6444	21.5 ± 8.2	33.7 ± 0.2	22.0%	1.07	1.039	$22.9 \pm 8.8 \pm 0.6 \pm 0.9$
2.6464	22.3 ± 8.4	34.0 ± 0.3	22.0%	1.07	1.039	$23.5 \pm 8.9 \pm 0.6 \pm 0.9$
2.9000	20.4 ± 9.1	105 ± 1	22.7%	1.08	1.033	$6.7 \pm 3.0 \pm 0.2 \pm 0.2$
2.9500	2.2 ± 1.1	15.9 ± 0.1	22.5%	1.08	1.029	$4.8 \pm 2.4 \pm 0.1 \pm 0.3$
2.9810	2.5 ± 1.1	16.1 ± 0.1	22.9%	1.08	1.025	$5.3 \pm 2.4 \pm 0.1 \pm 0.3$
3.0000	4.7 ± 2.2	15.9 ± 0.1	22.8%	1.08	1.021	$10.3 \pm 4.7 \pm 0.3 \pm 0.6$
3.0200	2.2 ± 1.1	17.3 ± 0.1	23.0%	1.08	1.014	$4.5 \pm 2.1 \pm 0.1 \pm 0.2$
3.0800	8.7 ± 3.7	126 ± 1	23.6%	1.08	0.915	$2.6 \pm 1.1 \pm 0.1 \pm 0.1$

Table 6. The measured Born cross sections for $e^+e^- \to K_2^*(1430)^0\bar{K}^0$, where the first uncertainties are statistical, the second ones are systematics from table 7 and the third ones are model uncertainties.

5. The uncertainty related to the kinematic fit is studied with a control sample of $J/\psi \to K_S^0 K_L^0 \pi^0$. The difference in efficiency between data and MC simulation with and without the kinematic fit is taken as the uncertainty.

6. The uncertainty of the VP and ISR correction factors (Rad) is obtained with the accuracy of the radiation function, which is about 0.5% [56], and has an additional contribution from the cross section line shape, which is estimated by varying the model parameters of the fit to the cross section. All parameters are randomly varied within their uncertainties, and the resulting parametrization of the line shape is used to recalculate $(1+\delta)\epsilon$ and the corresponding cross section. This procedure is repeated one thousand times, and the standard deviation of the resulting cross sections is taken as the systematic uncertainty. The systematic uncertainty associated with the VP and ISR correction factor is evaluated as the quadratic sum of contributions from the QED theory and line shape parametrization [10].

JHEP01(2024)180

7. The uncertainty associated with the BFs from the PDG [1] is 0.08%, including both $\mathcal{B}(K^0_S \to \pi^+\pi^-) = (69.20 \pm 0.05)\%$ and $\mathcal{B}(\pi^0 \to \gamma\gamma) = (98.823 \pm 0.034)\%$.

8. The uncertainty caused by the $M(\pi^+\pi^-)$ fit (Fit) includes the descriptions of signal shape and background shape. The nominal MC-simulated shape convolved with a Gaussian function is replaced by a MC-simulated shape convolved with a Crystal Ball function, and the nominal background shape is replaced by a second-order polynomial function, and the differences with the nominal results are taken as the uncertainties. The uncertainties from above sources are added in quadrature and taken as the total uncertainty from the $M(\pi^+\pi^-)$ fit.

The second category of uncertainties includes those associated with the PWA fit that are evaluated as follows:

1. The uncertainty from the fit parameters (FPar) is estimated by the standard deviation of re-calculated efficiencies derived from one thousand groups of randomly generated fit parameters using a correlated multi-variable Gaussian function.

2. The uncertainty related to the resonance parameters (Par) is estimated by performing alternative fits shifting the world-average parameter value by its error from the PDG [1].

3. The uncertainty concerning the extra additional resonances (Extra) is estimated by performing alternative fits with all components whose significances are greater than 3σ. In the alternative fit $K^*(1410)^0 \to K^0\pi^0$ is added for the data sample at $\sqrt{s} = 2.125\,\text{GeV}$, $K^*(1410)^0 \to K^0\pi^0$ and $\rho(1450) \to K^0\bar{K}^0$ are added at $\sqrt{s} = 2.396\,\text{GeV}$, $\rho(1450)/\rho(1700) \to K^0\bar{K}^0$ and $K^*(1410)^0/K^*_3(1780)^0 \to K^0\pi^0$ are added at $\sqrt{s} = 2.900\,\text{GeV}$.

4. The uncertainty of the background estimation in the PWA fit (Bkg) is estimated by using only the lower or higher sideband.

5. The uncertainty from the Blatt-Weisskopf barrier factor (BWf) is estimated by varying the radius of the centrifugal barrier from 0.7 to 1.0 fm.

Assuming all the sources of systematic uncertainties as independent, the total systematic uncertainty is obtained by adding them in quadrature. The 100% correlated uncertainties for the Born cross sections of $e^+e^- \to K^0_S K^0_L \pi^0$, $K^*(892)^0\bar{K}^0$ and $K^*_2(1430)^0\bar{K}^0$ are listed in table 7. The other uncorrelated and total systematic uncertainties are listed in tables 8–10.

7 Fit to the lineshape

The Born cross sections for the process $e^+e^- \to K^0_S K^0_L \pi^0$ are shown in figure 6(a). The results are consistent with the previous results from BaBar. The Born cross sections for the intermediate process $e^+e^- \to K^*_2(1430)^0\bar{K}^0$ and $e^+e^- \to K^*(892)^0\bar{K}^0$ are shown in figures 6(b) and 7, respectively.

A χ^2 fit, incorporating the correlated and uncorrelated uncertainties among different energy points, is performed to determine the resonance parameters for the Born cross sections

JHEP01(2024)180

Source	Uncertainty(%)
Luminosity	1.00
K^0_S reconstruction	1.00
Requirement on $N_{\rm charge}$	0.70
Photon reconstruction	2.00
Kinematic fit	0.70
BF	0.08
Total	2.63

Table 7. The 100% correlated systematic uncertainties for the Born cross section of $e^+e^- \to K^0_S K^0_L \pi^0$.

$\sqrt{s}$ (GeV)	Rad	Fit	FPar	Par	Extra	Bkg	BWf	Total
2.0000	0.50	0.91	2.40	0.70	0.41	0.26	0.21	2.76
2.0500	0.50	2.13	2.50	2.11	0.40	0.30	0.21	3.97
2.1000	0.50	0.36	2.40	1.02	0.40	0.30	0.17	2.73
2.1250	0.50	0.94	0.80	0.22	0.38	0.07	0.13	1.41
2.1500	0.50	2.83	2.60	1.10	0.43	0.30	0.31	4.07
2.1750	0.50	1.14	3.00	1.53	0.40	0.24	0.40	3.64
2.2000	0.50	1.39	2.50	1.11	0.41	0.30	0.22	3.16
2.2324	0.50	2.11	2.20	1.02	0.32	0.30	0.17	3.29
2.3094	0.50	2.71	2.40	1.10	0.31	0.28	0.22	3.84
2.3864	0.50	1.44	3.00	1.10	0.30	0.30	0.21	3.57
2.3960	0.50	1.36	1.40	0.60	0.30	0.15	0.21	2.14
2.6444	0.50	2.12	1.41	1.02	0.30	0.18	0.40	2.84
2.6464	0.50	2.05	1.40	1.02	0.30	0.18	0.40	2.78
2.9000	0.50	1.50	1.30	0.68	0.29	0.20	0.13	2.19
2.9500	0.51	3.20	2.57	2.10	0.33	0.30	0.31	4.67
2.9810	0.50	2.50	2.20	1.69	0.31	0.30	0.30	3.80
3.0000	0.50	3.75	2.20	2.06	0.30	0.28	0.25	4.86
3.0200	0.50	2.58	1.70	1.91	0.30	0.30	0.30	3.70
3.0800	0.50	0.98	1.70	1.02	0.31	0.20	0.20	2.30

Table 8. Systematic uncertainties (%) for the Born cross section of $e^+e^- \to K^0_S K^0_L \pi^0$ at each c.m. energy associated with the ISR and VP correction factors (Rad), the M($\pi^+\pi^-$) fit (Fit), the fit parameters in PWA (FPar), the resonance parameters (Par), the extra additional resonances (Extra), the background estimation (Bkg) and the Blatt-Weisskopf barrier factor (BWf).

JHEP01(2024)180

$\sqrt{s}$ (GeV)	Rad	Fit	Par	Extra	Bkg	BWf	Total
2.0000	0.50	0.91	1.90	0.71	1.43	1.91	3.30
2.0500	0.50	2.13	1.22	0.70	2.32	3.10	4.67
2.1000	0.50	0.36	1.71	0.70	1.72	2.01	3.29
2.1250	0.50	0.94	0.21	0.68	0.20	0.73	1.49
2.1500	0.50	2.83	1.23	0.73	1.30	2.01	4.00
2.1750	0.50	1.14	1.01	0.70	1.12	2.40	3.17
2.2000	0.50	1.39	1.32	0.71	1.52	2.22	3.42
2.2324	0.50	2.11	1.10	0.52	1.15	1.67	3.21
2.3094	0.50	2.71	1.05	0.51	1.09	1.42	3.49
2.3864	0.50	1.44	1.04	0.51	1.14	2.20	3.13
2.3960	0.50	1.36	0.53	0.50	0.50	1.13	2.03
2.6444	0.50	2.12	0.72	0.51	1.20	1.70	3.14
2.6464	0.50	2.05	0.72	0.51	1.17	1.70	3.08
2.9000	0.50	1.50	0.38	0.69	1.57	1.32	2.71
2.9500	0.51	3.20	3.01	0.73	2.31	3.18	5.96
2.9810	0.50	2.50	3.01	0.71	2.11	3.17	5.53
3.0000	0.50	3.75	1.53	0.70	2.01	2.68	5.33
3.0200	0.50	2.58	1.22	0.70	1.42	4.20	5.34
3.0800	0.50	0.98	0.50	0.71	0.97	1.27	2.13

Table 9. Systematic uncertainties (%) for the Born cross section of $e^+e^- \to K^*(892)^0\bar{K}^0$ at each c.m. energy associated with the ISR and VP correction factors (Rad), the M($\pi^+\pi^-$) fit (Fit), the fit parameters in PWA (FPar), the resonance parameters (Par), the extra additional resonances (Extra), the background estimation (Bkg) and the Blatt-Weisskopf barrier factor (BWf).

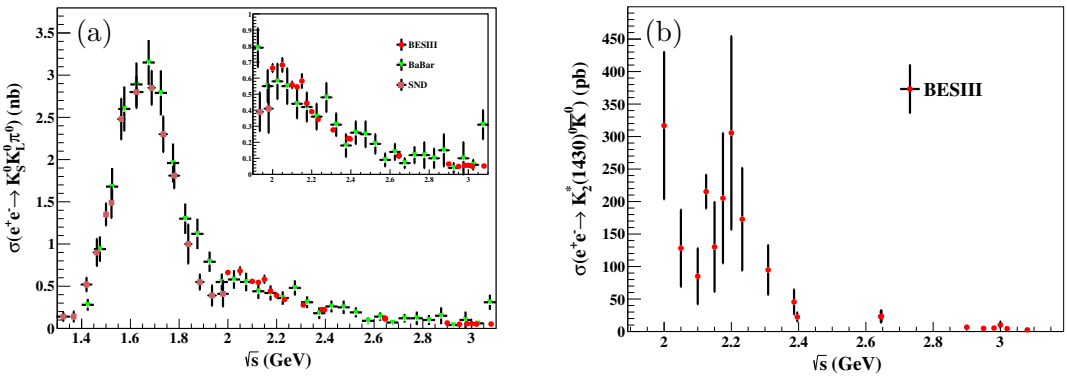

Figure 6. The Born cross sections for (a) the process $e^+e^- \to K^0_S K^0_L \pi^0$ and (b) the process $e^+e^- \to K^*_2(1430)^0\bar{K}^0$. The red dots are the measured results from BESIII, where errors include both statistical and systematic uncertainties. The green triangles and brown squares are the results from BaBar and SND, respectively.

JHEP01(2024)180

$\sqrt{s}$ (GeV)	Rad	Fit	Par	Extra	Bkg	BWf	Total
2.0000	0.50	0.91	2.02	1.00	1.50	2.07	3.56
2.0500	0.50	2.13	2.10	1.00	2.70	2.21	4.73
2.1000	0.50	0.36	2.27	1.00	2.58	2.21	4.25
2.1250	0.50	0.94	1.01	1.00	1.05	1.29	2.43
2.1500	0.50	2.83	1.82	1.00	2.22	2.08	4.67
2.1750	0.50	1.14	2.10	1.00	1.50	2.10	3.69
2.2000	0.50	1.39	2.10	1.00	1.92	2.21	4.02
2.2324	0.50	2.11	2.12	1.31	2.00	2.01	4.35
2.3094	0.50	2.71	2.10	1.30	1.50	2.10	4.51
2.3864	0.50	1.44	2.10	1.30	1.62	2.10	3.93
2.3960	0.50	1.36	1.49	1.31	1.31	1.70	3.26
2.6444	0.50	2.12	1.70	1.31	1.67	2.00	4.02
2.6464	0.50	2.05	1.70	1.31	1.70	2.00	3.99
2.9000	0.50	1.50	1.38	1.50	1.20	1.92	3.43
2.9500	0.51	3.20	2.50	1.53	2.00	2.20	5.28
2.9810	0.50	2.50	2.72	1.52	2.03	2.11	4.98
3.0000	0.50	3.75	2.51	1.52	2.11	2.20	5.68
3.0200	0.50	2.58	2.51	1.52	2.12	2.00	4.90
3.0800	0.50	0.98	1.70	1.51	1.20	1.92	3.39

Table 10. Systematic uncertainties (%) for the Born cross section of $e^+e^- \to K_2^*(1430)^0\bar{K}^0$ at each c.m. energy associated with the ISR and VP correction factors (Rad), the M($\pi^+\pi^-$) fit (Fit), the resonance parameters (Par), the extra additional resonances (Extra), the background estimation (Bkg) and the Blatt-Weisskopf barrier factor (BWf).

of $e^+e^- \to K^*(892)^0\bar{K}^0$. The fit probability density function is a coherent sum of a continuum component and a resonant component. The cross section is modeled as:

$$\sigma = |\frac{\sqrt{12\pi\Gamma_Y\Gamma_Y^{e^+e^-}\mathcal{B}}}{M_Y^2 - s - iM_Y\Gamma(\sqrt{s})}\sqrt{\frac{P(\sqrt{s})}{P(M_Y)}}e^{i\phi_Y} + c_1\frac{\sqrt{P(\sqrt{s})}}{s^{c_2}}|^2, \tag{7.1}$$

where M_Y and Γ_Y are the mass and width of the resonance; ϕ_Y is the relative phase between the continuum component and the resonance; $\Gamma_Y^{e^+e^-}$ is its partial width to e^+e^-; $\mathcal{B}$ is the BF of $Y \to K^*(892)^0\bar{K}^0$; and c_1 and c_2 are additional parameters of the fit. $\Gamma(\sqrt{s})$ is defined as $\Gamma_Y(\frac{P(\sqrt{s})}{P(M_Y)})$, where $P(\sqrt{s}) = \int\sum_m |A_{K^*(892)^0\bar{K}^0}(m)|^2 d\Phi_3$ is the phase-space factor for the relative orbital angular momentum $L = 1$ of the process $e^+e^- \to K^*(892)^0\bar{K}^0 \to K_S^0K_L^0\pi^0$ and Φ_3 is three-body phase space [1]. The amplitude A is the partial wave amplitude in the covariant Rarita-Schwinger tensor formalism [50] and is described as:

$$A_{K^*(892)^0\bar{K}^0}(m) = -Y^\mu(m)\epsilon_{\mu\nu\lambda\sigma}p^\sigma_{(K_S^0K_L^0\pi^0)}\tilde{T}^{(1)\nu}_{K^*(892)^0\bar{K}^0}\cdot f^{K^*(892)^0}_{K^0\pi^0}\cdot\tilde{T}^{(1)\lambda}_{K^0\pi^0}, \tag{7.2}$$

JHEP01(2024)180

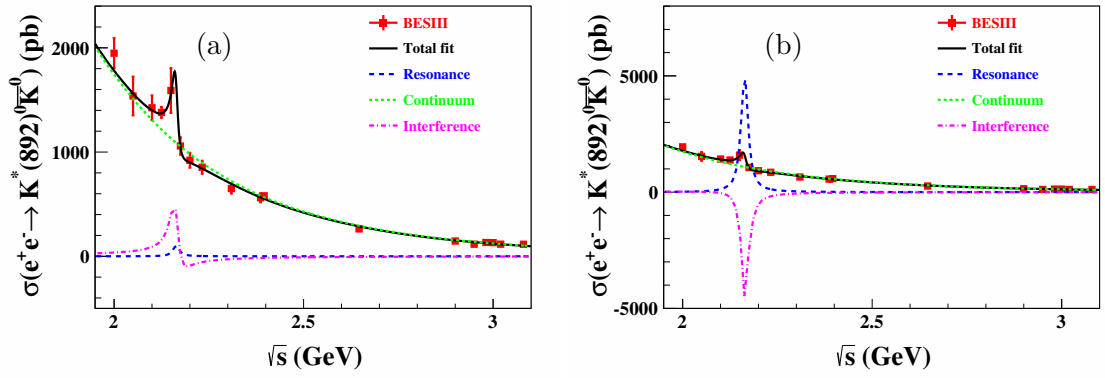

Figure 7. The Born cross section and fit curves for $e^+e^- \to K^*(892)^0\bar{K}^0$, (a) and (b), corresponding to the two solutions in table 11. Rectangles with error bars are BESIII data, where errors include both statistical and systematic uncertainties. The solid black curves represent the total fit result, the dashed blue curves for the resonance and the dashed green curves for the continuum component, and the dash-dotted pink curves for the interference between the resonance and continuum components.

where $\tilde{T}$ is the covariant tensor, f is the Breit-Wigner propagator, $\epsilon_{\mu\nu\lambda\sigma}$ is the Levi-Civita symbol, and the other operators can be found in ref. [50].

In total, there are six free parameters in the fit: $M_Y, \Gamma_Y, \phi_Y, c_1, c_2$ and the product of $\Gamma_Y^{e^+e^-}\mathcal{B}$. The fit results are shown in figure 7, and the resonance parameters are listed in table 11. The fit has $\chi^2/\text{ndf} = 18.95/13(p = 0.125)$ with two solutions for the resonance with identical mass and width, but different relative phase ϕ_Y and $\Gamma_Y^{e^+e^-}\mathcal{B}$. The mass and width of the resonance are $M_Y = (2164.1 \pm 9.6)$ MeV/c^2 and $\Gamma_Y = (32.4 \pm 21.1)$ MeV, respectively, including all sources of uncertainties from cross section measurement. The significance of the resonance is determined to be 3.2σ by comparing the change of χ^2 ($\Delta\chi^2 = 18.27$) and the change of ndf ($\Delta\text{ndf} = 4$) between the nominal fit and the fit without the resonance. As both solutions are mathematically equivalent, we do not prefer one over the other, but list them in order of increasing interference fraction. Figure 7(b) shows a large interference between resonance and continuum components. The uncertainties (statistical and systematic) of the measured Born cross sections have been included when fitting the line shape, determining the resonance parameters and estimating the significance of the resonance.

Besides the uncertainties of individual cross-section measurements, the fit to the lineshape is also affected by the uncertainty of the BEPCII c.m. energy and the description of the continuum. The uncertainty of the c.m. energy calibration is estimated as 0.1% and is ignored in the determination of resonance parameters [36]. To evaluate the systematic uncertainty associated with the lineshape model, the continuum term $c_1\frac{\sqrt{P(\sqrt{s})}}{s^{c_2}}$ is replaced with an exponential function of the form $c_0 \cdot e^{-p_0(\sqrt{s}-M_{th})}$, where c_0 and p_0 are free parameters and $M_{th} = m_{K^*(892)^0} + m_{\bar{K}^0}$ is the mass threshold for $K^*(892)^0\bar{K}^0$ production [1, 12]. The difference of the parameters from the nominal results are taken as the systematic uncertainties.

JHEP01(2024)180

Parameter	Solution 1	Solution 2
$M_Y(\mathrm{MeV}/c^2)$	$2164.7 \pm 9.1 \pm 3.1$	
$\Gamma_Y(\mathrm{MeV})$	$32.4 \pm 21.0 \pm 1.8$	
$\Gamma_Y^{e^+e^-}\mathcal{B}(\mathrm{eV})$	$1.0 \pm 0.2 \pm 0.1$	$73.6 \pm 4.4 \pm 2.0$
$\phi_Y(\mathrm{rad})$	$2.5 \pm 0.5 \pm 0.1$	$-1.7 \pm 0.1 \pm 0.1$
Significance	3.2σ	

Table 11. Result of the fit to the $e^+e^- \to K^*(892)^0\bar{K}^0$ Born cross sections, where the first uncertainties originate from the cross section measurement and the second from the line shape fit methodology, respectively.

8 Summary

In summary, a partial wave analysis of the process $e^+e^- \to K_S^0K_L^0\pi^0$ is performed for nineteen data samples collected in the BESIII experiment with center-of-mass energies ranging from 2.000 to 3.080 GeV corresponding to a total integrated luminosity of 647 pb^{-1}. The Born cross sections of the process $e^+e^- \to K_S^0K_L^0\pi^0$, as well as those for the intermediate processes $e^+e^- \to K^*(892)^0\bar{K}^0$ and $K_2^*(1430)^0\bar{K}^0$ are measured by performing partial wave analysis on each data sample individually, where the charge conjugated processes are also included. The measured Born cross sections of the process $e^+e^- \to K_S^0K_L^0\pi^0$ are consistent with earlier results by BaBar [34], while the precision is significantly improved. The Born cross section lineshape of the process $e^+e^- \to K^*(892)^0\bar{K}^0$ hints at a resonant structure around 2.2 GeV with a significance of 3.2σ. A Breit-Wigner fit yields its mass $M_Y = (2164.7\pm9.1\pm3.1)$ MeV/c^2 and width $\Gamma_Y = (32.4 \pm 21.0 \pm 1.8)$ MeV. The resonance parameters, especially the very narrow width, are very close to the BESIII results measured through the $\phi\eta$ channel [7] of the $\phi(2170)$ meson [1].

The ratio of Born cross section measurements of the process $e^+e^- \to K^*(892)^+K^-$ to the process $e^+e^- \to K^*(892)^0\bar{K}^0$ is less than 0.2 and that for $K_2^*(1430)$ is in the region of 0-40, where the statistical and systematic uncertainties are included. If we apply the isospin decomposition for the decay from isospin vector (ρ^*) or isospin scalar (ω^*, ϕ^*) state to the final state $K^*\bar{K}$, the ratio of the yields in the neutral and charged $K^*\bar{K}$ should be 1. On the other hand, the electromagnetic interaction also contributes to the production of $e^+e^- \to K^*\bar{K}$, and it does not require isospin conservation. Future experimental and theoretical studies are needed to understand the observed phenomenon.

Acknowledgments

The BESIII Collaboration thanks the staff of BEPCII, the IHEP computing center and the supercomputing center of USTC for their strong support. This work is supported in part by National Key R&D Program of China under Contracts Nos. 2020YFA0406400, 2020YFA0406300; National Natural Science Foundation of China (NSFC) under Contracts Nos. 11635010, 11735014, 11835012, 11935015, 11935016, 11935018, 11961141012, 12022510, 12025502, 12035009, 12035013, 12192260, 12192261, 12192262, 12192263, 12192264, 12192265,

JHEP01(2024)180

12275320, 11625523, 11705192, 11950410506, 12061131003, 12105276, 12122509, 12205255; the Chinese Academy of Sciences (CAS) Large-Scale Scientific Facility Program; the CAS Center for Excellence in Particle Physics (CCEPP); Joint Large-Scale Scientific Facility Funds of the NSFC and CAS under Contracts Nos. U1832207, U1732263, U1832103, U2032111; CAS Key Research Program of Frontier Sciences under Contracts Nos. QYZDJ-SSW-SLH003, QYZDJ-SSW-SLH040; 100 Talents Program of CAS; The Institute of Nuclear and Particle Physics (INPAC) and Shanghai Key Laboratory for Particle Physics and Cosmology; ERC under Contract No. 758462; European Union's Horizon 2020 research and innovation programme under Marie Sklodowska-Curie grant agreement under Contract No. 894790; German Research Foundation DFG under Contracts Nos. 443159800, 455635585, Collaborative Research Center CRC 1044, FOR5327, GRK 2149; Istituto Nazionale di Fisica Nucleare, Italy; Ministry of Development of Turkey under Contract No. DPT2006K-120470; National Research Foundation of Korea under Contract No. NRF-2022R1A2C1092335; National Science and Technology fund; National Science Research and Innovation Fund (NSRF) via the Program Management Unit for Human Resources & Institutional Development, Research and Innovation under Contract No. B16F640076; Polish National Science Centre under Contract No. 2019/35/O/ST2/02907; The Royal Society, U.K. under Contracts Nos. DH140054, DH160214; The Swedish Research Council; U.S. Department of Energy under Contract No. DE-FG02-05ER41374.

References

[1] Particle Data Group collaboration, *Review of particle physics*, *PTEP* **2022** (2022) 083C01 [INSPIRE].

[2] BaBar collaboration, *A structure at* 2175 *MeV in* $e^+e^- \to \phi f_0(980)$ *observed via initial-state radiation*, *Phys. Rev. D* **74** (2006) 091103 [hep-ex/0610018] [INSPIRE].

[3] Belle collaboration, *Observation of the* $\phi(1680)$ *and the* $Y(2175)$ *in* $e^+e^- \to \phi\pi^+\pi^-$, *Phys. Rev. D* **80** (2009) 031101 [arXiv:0808.0006] [INSPIRE].

[4] BES collaboration, *Observation of* $Y(2175)$ *in* $J/\psi \to \eta\phi f_0(980)$, *Phys. Rev. Lett.* **100** (2008) 102003 [arXiv:0712.1143] [INSPIRE].

[5] BESIII collaboration, *Study of* $J/\psi \to \eta\phi\pi^+\pi^-$ *at BESIII*, *Phys. Rev. D* **91** (2015) 052017 [arXiv:1412.5258] [INSPIRE].

[6] BESIII collaboration, *Observation of* $e^+e^- \to \eta Y(2175)$ *at center-of-mass energies above* 3.7 *GeV*, *Phys. Rev. D* **99** (2019) 012014 [arXiv:1709.04323] [INSPIRE].

[7] BESIII collaboration, *Study of the process* $e^+e^- \to \phi\eta$ *at center-of-mass energies between* 2.00 *and* 3.08 *GeV*, *Phys. Rev. D* **104** (2021) 032007 [arXiv:2104.05549] [INSPIRE].

[8] BESIII collaboration, *Observation of a structure in* $e^+e^- \to \phi\eta'$ *at* $\sqrt{s}$ *from* 2.05 *to* 3.08 *GeV*, *Phys. Rev. D* **102** (2020) 012008 [arXiv:2003.13064] [INSPIRE].

[9] BESIII collaboration, *Measurement of* $e^+e^- \to \phi\pi^+\pi^-$ *cross sections at center-of-mass energies from* 2.00 *to* 3.08 *GeV*, *Phys. Rev. D* **108** (2023) 032011 [arXiv:2112.13219] [INSPIRE].

JHEP01(2024)180

[10] BESIII collaboration, *Measurement of $e^+e^- \to K^+K^-$ cross section at $\sqrt{s} = 2.00$–3.08 GeV*, *Phys. Rev. D* **99** (2019) 032001 [arXiv:1811.08742] [INSPIRE].

[11] BESIII collaboration, *Cross section measurement of $e^+e^- \to K^0_S K^0_L$ at $\sqrt{s} = 2.00$–3.08 GeV*, *Phys. Rev. D* **104** (2021) 092014 [arXiv:2105.13597] [INSPIRE].

[12] BESIII collaboration, *Measurement of $e^+e^- \to K^+K^-\pi^0$ cross section and observation of a resonant structure*, *JHEP* **07** (2022) 045 [arXiv:2202.06447] [INSPIRE].

[13] BESIII collaboration, *Observation of a resonant structure in $e^+e^- \to K^+K^-\pi^0\pi^0$*, *Phys. Rev. Lett.* **124** (2020) 112001 [arXiv:2001.04131] [INSPIRE].

[14] T. Barnes, N. Black and P.R. Page, *Strong decays of strange quarkonia*, *Phys. Rev. D* **68** (2003) 054014 [nucl-th/0208072] [INSPIRE].

[15] G.-J. Ding and M.-L. Yan, *$Y(2175)$: distinguish hybrid state from higher quarkonium*, *Phys. Lett. B* **657** (2007) 49 [hep-ph/0701047] [INSPIRE].

[16] X. Wang et al., *Non-strange partner of strangeonium-like state $Y(2175)$*, *Phys. Rev. D* **85** (2012) 074024 [arXiv:1202.4139] [INSPIRE].

[17] S.S. Afonin and I.V. Pusenkov, *Universal description of radially excited heavy and light vector mesons*, *Phys. Rev. D* **90** (2014) 094020 [arXiv:1411.2390] [INSPIRE].

[18] G.-J. Ding and M.-L. Yan, *A candidate for 1^- strangeonium hybrid*, *Phys. Lett. B* **650** (2007) 390 [hep-ph/0611319] [INSPIRE].

[19] P.R. Page, E.S. Swanson and A.P. Szczepaniak, *Hybrid meson decay phenomenology*, *Phys. Rev. D* **59** (1999) 034016 [hep-ph/9808346] [INSPIRE].

[20] Z.-G. Wang, *Analysis of the $Y(2175)$ as a tetraquark state with QCD sum rules*, *Nucl. Phys. A* **791** (2007) 106 [hep-ph/0610171] [INSPIRE].

[21] H.-X. Chen, X. Liu, A. Hosaka and S.-L. Zhu, *The $Y(2175)$ state in the QCD sum rule*, *Phys. Rev. D* **78** (2008) 034012 [arXiv:0801.4603] [INSPIRE].

[22] H.-W. Ke and X.-Q. Li, *Study of the strong decays of $\phi(2170)$ and the future charm-tau factory*, *Phys. Rev. D* **99** (2019) 036014 [arXiv:1810.07912] [INSPIRE].

[23] N.V. Drenska, R. Faccini and A.D. Polosa, *Higher tetraquark particles*, *Phys. Lett. B* **669** (2008) 160 [arXiv:0807.0593] [INSPIRE].

[24] L. Zhao, N. Li, S.-L. Zhu and B.-S. Zou, *Meson-exchange model for the $\Lambda\bar{\Lambda}$ interaction*, *Phys. Rev. D* **87** (2013) 054034 [arXiv:1302.1770] [INSPIRE].

[25] C. Deng, J. Ping, Y. Yang and F. Wang, *Baryonia and near-threshold enhancements*, *Phys. Rev. D* **88** (2013) 074007 [arXiv:1306.6725] [INSPIRE].

[26] Y. Dong et al., *Selected strong decays of $\eta(2225)$ and $\phi(2170)$ as $\Lambda\bar{\Lambda}$ bound states*, *Phys. Rev. D* **96** (2017) 074027 [arXiv:1705.09631] [INSPIRE].

[27] S. Gomez-Avila, M. Napsuciale and E. Oset, *ϕK^+K^- production in electron-positron annihilation*, *Phys. Rev. D* **79** (2009) 034018 [arXiv:0711.4147] [INSPIRE].

[28] BaBar collaboration, *Measurements of $e^+e^- \to K^+K^-\eta$, $K^+K^-\pi^0$ and $K^0_s K^\pm\pi^\mp$ cross-sections using initial state radiation events*, *Phys. Rev. D* **77** (2008) 092002 [arXiv:0710.4451] [INSPIRE].

[29] BaBar collaboration, *The $e^+e^- \to K^+K^-\pi^+\pi^-$, $K^+K^-\pi^0\pi^0$ and $K^+K^-K^+K^-$ cross-sections measured with initial-state radiation*, *Phys. Rev. D* **76** (2007) 012008 [arXiv:0704.0630] [INSPIRE].

JHEP01(2024)180

[30] BaBar collaboration, *Precision measurement of the $e^+e^- \to K^+K^-(\gamma)$ cross section with the initial-state radiation method at BABAR*, *Phys. Rev. D* **88** (2013) 032013 [arXiv:1306.3600] [INSPIRE].

[31] BaBar collaboration, *Resonances in e^+e^- annihilation near 2.2 GeV*, *Phys. Rev. D* **101** (2020) 012011 [arXiv:1912.04512] [INSPIRE].

[32] BaBar collaboration, *Cross sections for the reactions $e^+e^- \to K^0_S K^0_L$, $K^0_S K^0_L \pi^+\pi^-$, $K^0_S K^0_S \pi^+\pi^-$, and $K^0_S K^0_S K^+K^-$ from events with initial-state radiation*, *Phys. Rev. D* **89** (2014) 092002 [arXiv:1403.7593] [INSPIRE].

[33] Y. Ma, Y. Chen, M. Gong and Z. Liu, *Strangeonium-like hybrids on the lattice*, *Chin. Phys. C* **45** (2021) 013112 [arXiv:2007.14893] [INSPIRE].

[34] BaBar collaboration, *Cross sections for the reactions $e^+e^- \to K^0_S K^0_L \pi^0$, $K^0_S K^0_L \eta$, and $K^0_S K^0_L \pi^0\pi^0$ from events with initial-state radiation*, *Phys. Rev. D* **95** (2017) 052001 [arXiv:1701.08297] [INSPIRE].

[35] M.N. Achasov et al., *Measurement of the $e^+e^- \to K_S K_L \pi^0$ cross section in the energy range $\sqrt{s} = 1.3$–2.0 GeV*, *Phys. Rev. D* **97** (2018) 032011 [arXiv:1711.07143] [INSPIRE].

[36] BESIII collaboration, *Luminosity measurements for the R scan experiment at BESIII*, *Chin. Phys. C* **41** (2017) 063001 [arXiv:1702.04977] [INSPIRE].

[37] BESIII collaboration, *Measurement of $e^+e^- \to \omega\pi^+\pi^-$ cross section at $\sqrt{s} = 2.000$ to 3.080 GeV*, *JHEP* **01** (2023) 111 [*Erratum ibid.* **03** (2023) 093] [arXiv:2208.04507] [INSPIRE].

[38] BESIII collaboration, *Design and construction of the BESIII detector*, *Nucl. Instrum. Meth. A* **614** (2010) 345 [arXiv:0911.4960] [INSPIRE].

[39] C. Yu et al., *BEPCII performance and beam dynamics studies on luminosity*, in the proceedings of the 7th *International Particle Accelerator Conference*, (2016), p. TUYA01 [DOI:10.18429/JACoW-IPAC2016-TUYA01] [INSPIRE].

[40] BESIII collaboration, *Future physics programme of BESIII*, *Chin. Phys. C* **44** (2020) 040001 [arXiv:1912.05983] [INSPIRE].

[41] GEANT4 collaboration, *GEANT4 — a simulation toolkit*, *Nucl. Instrum. Meth. A* **506** (2003) 250 [INSPIRE].

[42] K.-X. Huang et al., *Method for detector description transformation to Unity and application in BESIII*, *Nucl. Sci. Tech.* **33** (2022) 142 [arXiv:2206.10117] [INSPIRE].

[43] R.-G. Ping, *An exclusive event generator for e^+e^- scan experiments*, *Chin. Phys. C* **38** (2014) 083001 [arXiv:1309.3932] [INSPIRE].

[44] B. Andersson and H.-M. Hu, *Few body states in Lund string fragmentation model*, hep-ph/9910285 [INSPIRE].

[45] H. Czyż, P. Kisza and S. Tracz, *Modeling interactions of photons with pseudoscalar and vector mesons*, *Phys. Rev. D* **97** (2018) 016006 [arXiv:1711.00820] [INSPIRE].

[46] BaBar collaboration, *Measurement of the $e^+e^- \to \pi^+\pi^-\pi^0\pi^0$ cross section using initial-state radiation at BABAR*, *Phys. Rev. D* **96** (2017) 092009 [arXiv:1709.01171] [INSPIRE].

[47] BaBar collaboration, *Measurement of the $e^+e^- \to K^0_S K^\pm \pi^\mp \pi^0$ and $K^0_S K^\pm \pi^\mp \eta$ cross sections using initial-state radiation*, *Phys. Rev. D* **95** (2017) 092005 [arXiv:1704.05009] [INSPIRE].

[48] A. Rogozhnikov, *Reweighting with boosted decision trees*, *J. Phys. Conf. Ser.* **762** (2016) 012036 [arXiv:1608.05806] [INSPIRE].

JHEP01(2024)180

[49] N. Berger, B. Liu and J. Wang, *Partial wave analysis using graphics processing units*, *J. Phys. Conf. Ser.* **219** (2010) 042031 [INSPIRE].

[50] B.S. Zou and D.V. Bugg, *Covariant tensor formalism for partial wave analyses of ψ decay to mesons*, *Eur. Phys. J. A* **16** (2003) 537 [hep-ph/0211457] [INSPIRE].

[51] W. Rarita and J. Schwinger, *On a theory of particles with half integral spin*, *Phys. Rev.* **60** (1941) 61 [INSPIRE].

[52] C. Zemach, *Use of angular momentum tensors*, *Phys. Rev.* **140** (1965) B97 [INSPIRE].

[53] S.U. Chung, *A general formulation of covariant helicity coupling amplitudes*, *Phys. Rev. D* **57** (1998) 431 [INSPIRE].

[54] J.H. Kuhn and A. Santamaria, *Tau decays to pions*, *Z. Phys. C* **48** (1990) 445 [INSPIRE].

[55] F. James and M. Roos, *Minuit: a system for function minimization and analysis of the parameter errors and correlations*, *Comput. Phys. Commun.* **10** (1975) 343 [INSPIRE].

[56] Working Group on Radiative Corrections and Monte Carlo Generators for Low Energies collaborations, *Quest for precision in hadronic cross sections at low energy: Monte Carlo tools vs. experimental data*, *Eur. Phys. J. C* **66** (2010) 585 [arXiv:0912.0749] [INSPIRE].

[57] E.A. Kuraev and V.S. Fadin, *On radiative corrections to e^+e^- single photon annihilation at high-energy*, *Sov. J. Nucl. Phys.* **41** (1985) 466 [INSPIRE].

[58] W. Sun et al., *An iterative weighting method to apply ISR correction to e^+e^- hadronic cross-section measurements*, *Front. Phys. (Beijing)* **16** (2021) 64501 [arXiv:2011.07889] [INSPIRE].

[59] BESIII collaboration, *Study of $\eta(1405)/\eta(1475)$ in $J/\psi \to \gamma K_S^0 K_S^0 \pi^0$ decay*, *JHEP* **03** (2023) 121 [arXiv:2209.11175] [INSPIRE].

[60] BESIII collaboration, *Branching fraction measurements of χ_{c0} and χ_{c2} to $\pi^0\pi^0$ and $\eta\eta$*, *Phys. Rev. D* **81** (2010) 052005 [arXiv:1001.5360] [INSPIRE].

JHEP01(2024)180

The BESIII collaboration

M. Ablikim[1], M.N. Achasov[5,b], P. Adlarson[75], X.C. Ai[81], R. Aliberti[36], A. Amoroso[74A,74C], M.R. An[40], Q. An[71,58], Y. Bai[57], O. Bakina[37], I. Balossino[30A], Y. Ban[47,g], V. Batozskaya[1,45], K. Begzsuren[33], N. Berger[36], M. Berlowski[45], M. Bertani[29A], D. Bettoni[30A], F. Bianchi[74A,74C], E. Bianco[74A,74C], A. Bortone[74A,74C], I. Boyko[37], R.A. Briere[6], A. Brueggemann[68], H. Cai[76], X. Cai[1,58], A. Calcaterra[29A], G.F. Cao[1,63], N. Cao[1,63], S.A. Cetin[62A], J.F. Chang[1,58], T.T. Chang[77], W.L. Chang[1,63], G.R. Che[44], G. Chelkov[37,a], C. Chen[44], Chao Chen[55], G. Chen[1], H.S. Chen[1,63], M.L. Chen[1,58,63], S.J. Chen[43], S.L. Chen[46], S.M. Chen[61], T. Chen[1,63], X.R. Chen[32,63], X.T. Chen[1,63], Y.B. Chen[1,58], Y.Q. Chen[35], Z.J. Chen[26,h], W.S. Cheng[74C], S.K. Choi[11], X. Chu[44], G. Cibinetto[30A], S.C. Coen[4], F. Cossio[74C], J.J. Cui[50], H.L. Dai[1,58], J.P. Dai[79], A. Dbeyssi[19], R. E. de Boer[4], D. Dedovich[37], Z.Y. Deng[1], A. Denig[36], I. Denysenko[37], M. Destefanis[74A,74C], F. De Mori[74A,74C], B. Ding[66,1], X.X. Ding[47,g], Y. Ding[35], Y. Ding[41], J. Dong[1,58], L.Y. Dong[1,63], M.Y. Dong[1,58,63], X. Dong[76], M.C. Du[1], S.X. Du[81], Z.H. Duan[43], P. Egorov[37,a], Y.H. Fan[46], J. Fang[1,58], S.S. Fang[1,63], W.X. Fang[1], Y. Fang[1], R. Farinelli[30A], L. Fava[74B,74C], F. Feldbauer[4], G. Felici[29A], C.Q. Feng[71,58], J.H. Feng[59], K Fischer[69], M. Fritsch[4], C.D. Fu[1], J.L. Fu[63], Y.W. Fu[1], H. Gao[63], Y.N. Gao[47,g], Yang Gao[71,58], S. Garbolino[74C], I. Garzia[30A,30B], P.T. Ge[76], Z.W. Ge[43], C. Geng[59], E.M. Gersabeck[67], A Gilman[69], K. Goetzen[14], L. Gong[41], W.X. Gong[1,58], W. Gradl[36], S. Gramigna[30A,30B], M. Greco[74A,74C], M.H. Gu[1,58], Y.T. Gu[16], C. Y Guan[1,63], Z.L. Guan[23], A.Q. Guo[32,63], L.B. Guo[42], M.J. Guo[50], R.P. Guo[49], Y.P. Guo[13,f], A. Guskov[37,a], T.T. Han[50], W.Y. Han[40], X.Q. Hao[20], F.A. Harris[65], K.K. He[55], K.L. He[1,63], F. H. H. Heinsius[4], C.H. Heinz[36], Y.K. Heng[1,58,63], C. Herold[60], T. Holtmann[4], P.C. Hong[13,f], G.Y. Hou[1,63], X.T. Hou[1,63], Y.R. Hou[63], Z.L. Hou[1], H.M. Hu[1,63], J.F. Hu[56,i], T. Hu[1,58,63], Y. Hu[1], G.S. Huang[71,58], K.X. Huang[59], L.Q. Huang[32,63], X.T. Huang[50], Y.P. Huang[1], T. Hussain[73], N Hüsken[28,36], N. in der Wiesche[68], M. Irshad[71,58], J. Jackson[28], S. Jaeger[4], S. Janchiv[33], J.H. Jeong[11], Q. Ji[1], Q.P. Ji[20], X.B. Ji[1,63], X.L. Ji[1,58], Y.Y. Ji[50], X.Q. Jia[50], Z.K. Jia[71,58], H.J. Jiang[76], P.C. Jiang[47,g], S.S. Jiang[40], T.J. Jiang[17], X.S. Jiang[1,58,63], Y. Jiang[63], J.B. Jiao[50], Z. Jiao[24], S. Jin[43], Y. Jin[66], M.Q. Jing[1,63], T. Johansson[75], X. Kui[1], S. Kabana[34], N. Kalantar-Nayestanaki[64], X.L. Kang[10], X.S. Kang[41], M. Kavatsyuk[64], B.C. Ke[81], A. Khoukaz[68], R. Kiuchi[1], R. Kliemt[14], O.B. Kolcu[62A], B. Kopf[4], M. Kuessner[4], A. Kupsc[45,75], W. Kühn[38], J.J. Lane[67], P. Larin[19], A. Lavania[27], L. Lavezzi[74A,74C], T.T. Lei[71,58], Z.H. Lei[71,58], H. Leithoff[36], M. Lellmann[36], T. Lenz[36], C. Li[44], C. Li[48], C.H. Li[40], Cheng Li[71,58], D.M. Li[81], F. Li[1,58], G. Li[1], H. Li[71,58], H.B. Li[1,63], H.J. Li[20], H.N. Li[56,i], Hui Li[44], J.R. Li[61], J.S. Li[59], J.W. Li[50], K.L. Li[20], Ke Li[1], L. J Li[1,63], L.K. Li[1], Lei Li[3], M.H. Li[44], P.R. Li[39,j,k], Q.X. Li[50], S.X. Li[13], T. Li[50], W.D. Li[1,63], W.G. Li[1], X.H. Li[71,58], X.L. Li[50], Xiaoyu Li[1,63], Y.G. Li[47,g], Z.J. Li[59], Z.X. Li[16], C. Liang[43], H. Liang[1,63], H. Liang[35], H. Liang[71,58], Y.F. Liang[54], Y.T. Liang[32,63], G.R. Liao[15], L.Z. Liao[50], Y.P. Liao[1,63], J. Libby[27], A. Limphirat[60], D.X. Lin[32,63], T. Lin[1], B.J. Liu[1], B.X. Liu[76], C. Liu[35], C.X. Liu[1], F.H. Liu[53], Fang Liu[1], Feng Liu[7], G.M. Liu[56,i], H. Liu[39,j,k], H.B. Liu[16], H.M. Liu[1,63], Huanhuan Liu[1], Huihui Liu[22], J.B. Liu[71,58], J.L. Liu[72], J.Y. Liu[1,63], K. Liu[1], K.Y. Liu[41], Ke Liu[23], L. Liu[71,58], L.C. Liu[44], Lu Liu[44], M.H. Liu[13,f], P.L. Liu[1], Q. Liu[63], S.B. Liu[71,58], T. Liu[13,f], W.K. Liu[44], W.M. Liu[71,58], X. Liu[39,j,k], Y. Liu[39,j,k], Y. Liu[81], Y.B. Liu[44], Z.A. Liu[1,58,63], Z.Q. Liu[50], X.C. Lou[1,58,63], F.X. Lu[59], H.J. Lu[24], J.G. Lu[1,58], X.L. Lu[1], Y. Lu[8], Y.P. Lu[1,58], Z.H. Lu[1,63], C.L. Luo[42], M.X. Luo[80], T. Luo[13,f], X.L. Luo[1,58], X.R. Lyu[63], Y.F. Lyu[44], F.C. Ma[41], H.L. Ma[1], J.L. Ma[1,63], L.L. Ma[50], M.M. Ma[1,63], Q.M. Ma[1], R.Q. Ma[1,63], R.T. Ma[63], X.Y. Ma[1,58], Y. Ma[47,g], Y.M. Ma[32], F.E. Maas[19],

JHEP01(2024)180

M. Maggiora[74A,74C], S. Malde[69], Q.A. Malik[73], A. Mangoni[29B], Y.J. Mao[47,g], Z.P. Mao[1], S. Marcello[74A,74C], Z.X. Meng[66], J.G. Messchendorp[14,64], G. Mezzadri[30A], H. Miao[1,63], T.J. Min[43], R.E. Mitchell[28], X.H. Mo[1,58,63], N. Yu. Muchnoi[5,b], J. Muskalla[36], Y. Nefedov[37], F. Nerling[19,d], I.B. Nikolaev[5,b], Z. Ning[1,58], S. Nisar[12,l], Q.L. Niu[39,j,k], W.D. Niu[55], Y. Niu [50], S.L. Olsen[63], Q. Ouyang[1,58,63], S. Pacetti[29B,29C], X. Pan[55], Y. Pan[57], A. Pathak[35], P. Patteri[29A], Y.P. Pei[71,58], M. Pelizaeus[4], H.P. Peng[71,58], Y.Y. Peng[39,j,k], K. Peters[14,d], J.L. Ping[42], R.G. Ping[1,63], S. Plura[36], V. Prasad[34], F.Z. Qi[1], H. Qi[71,58], H.R. Qi[61], M. Qi[43], T.Y. Qi[13,f], S. Qian[1,58], W.B. Qian[63], C.F. Qiao[63], J.J. Qin[72], L.Q. Qin[15], X.P. Qin[13,f], X.S. Qin[50], Z.H. Qin[1,58], J.F. Qiu[1], S.Q. Qu[61], C.F. Redmer[36], K.J. Ren[40], A. Rivetti[74C], M. Rolo[74C], G. Rong[1,63], Ch. Rosner[19], S.N. Ruan[44], N. Salone[45], A. Sarantsev[37,c], Y. Schelhaas[36], K. Schoenning[75], M. Scodeggio[30A,30B], K.Y. Shan[13,f], W. Shan[25], X.Y. Shan[71,58], J.F. Shangguan[55], L.G. Shao[1,63], M. Shao[71,58], C.P. Shen[13,f], H.F. Shen[1,63], W.H. Shen[63], X.Y. Shen[1,63], B.A. Shi[63], H.C. Shi[71,58], J.L. Shi[13], J.Y. Shi[1], Q.Q. Shi[55], R.S. Shi[1,63], X. Shi[1,58], J.J. Song[20], T.Z. Song[59], W.M. Song[35,1], Y. J. Song[13], Y.X. Song[47,g], S. Sosio[74A,74C], S. Spataro[74A,74C], F. Stieler[36], Y.J. Su[63], G.B. Sun[76], G.X. Sun[1], H. Sun[63], H.K. Sun[1], J.F. Sun[20], K. Sun[61], L. Sun[76], S.S. Sun[1,63], T. Sun[1,63], W.Y. Sun[35], Y. Sun[10], Y.J. Sun[71,58], Y.Z. Sun[1], Z.T. Sun[50], Y.X. Tan[71,58], C.J. Tang[54], G.Y. Tang[1], J. Tang[59], Y.A. Tang[76], L. Y Tao[72], Q.T. Tao[26,h], M. Tat[69], J.X. Teng[71,58], V. Thoren[75], W.H. Tian[59], W.H. Tian[52], Y. Tian[32,63], Z.F. Tian[76], I. Uman[62B], S.J. Wang[50], B. Wang[1], B.L. Wang[63], Bo Wang[71,58], C.W. Wang[43], D.Y. Wang[47,g], F. Wang[72], H.J. Wang[39,j,k], H.P. Wang[1,63], J.P. Wang [50], K. Wang[1,58], L.L. Wang[1], M. Wang[50], Meng Wang[1,63], S. Wang[13,f], S. Wang[39,j,k], T. Wang[13,f], T.J. Wang[44], W. Wang[72], W. Wang[59], W.P. Wang[71,58], X. Wang[47,g], X.F. Wang[39,j,k], X.J. Wang[40], X.L. Wang[13,f], Y. Wang[61], Y.D. Wang[46], Y.F. Wang[1,58,63], Y.H. Wang[48], Y.N. Wang[46], Y.Q. Wang[1], Yaqian Wang[18,1], Yi Wang[61], Z. Wang[1,58], Z.L. Wang[72], Z.Y. Wang[1,63], Ziyi Wang[63], D. Wei[70], D.H. Wei[15], F. Weidner[68], S.P. Wen[1], C.W. Wenzel[4], U. Wiedner[4], G. Wilkinson[69], M. Wolke[75], L. Wollenberg[4], C. Wu[40], J.F. Wu[1,63], L.H. Wu[1], L.J. Wu[1,63], X. Wu[13,f], X.H. Wu[35], Y. Wu[71], Y.H. Wu[55], Y.J. Wu[32], Z. Wu[1,58], L. Xia[71,58], X.M. Xian[40], T. Xiang[47,g], D. Xiao[39,j,k], G.Y. Xiao[43], S.Y. Xiao[1], Y. L. Xiao[13,f], Z.J. Xiao[42], C. Xie[43], X.H. Xie[47,g], Y. Xie[50], Y.G. Xie[1,58], Y.H. Xie[7], Z.P. Xie[71,58], T.Y. Xing[1,63], C.F. Xu[1,63], C.J. Xu[59], G.F. Xu[1], H.Y. Xu[66], Q.J. Xu[17], Q.N. Xu[31], W. Xu[1,63], W.L. Xu[66], X.P. Xu[55], Y.C. Xu[78], Z.P. Xu[43], Z.S. Xu[63], F. Yan[13,f], L. Yan[13,f], W.B. Yan[71,58], W.C. Yan[81], X.Q. Yan[1], H.J. Yang[51,e], H.L. Yang[35], H.X. Yang[1], Tao Yang[1], Y. Yang[13,f], Y.F. Yang[44], Y.X. Yang[1,63], Yifan Yang[1,63], Z.W. Yang[39,j,k], Z.P. Yao[50], M. Ye[1,58], M.H. Ye[9], J.H. Yin[1], Z.Y. You[59], B.X. Yu[1,58,63], C.X. Yu[44], G. Yu[1,63], J.S. Yu[26,h], T. Yu[72], X.D. Yu[47,g], C.Z. Yuan[1,63], L. Yuan[2], S.C. Yuan[1], X.Q. Yuan[1], Y. Yuan[1,63], Z.Y. Yuan[59], C.X. Yue[40], A.A. Zafar[73], F.R. Zeng[50], X. Zeng[13,f], Y. Zeng[26,h], Y.J. Zeng[1,63], X.Y. Zhai[35], Y.C. Zhai[50], Y.H. Zhan[59], A.Q. Zhang[1,63], B.L. Zhang[1,63], B.X. Zhang[1], D.H. Zhang[44], G.Y. Zhang[20], H. Zhang[71], H.C. Zhang[1,58,63], H.H. Zhang[59], H.H. Zhang[35], H.Q. Zhang[1,58,63], H.Y. Zhang[1,58], J. Zhang[81], J.J. Zhang[52], J.L. Zhang[21], J.Q. Zhang[42], J.W. Zhang[1,58,63], J.X. Zhang[39,j,k], J.Y. Zhang[1], J.Z. Zhang[1,63], Jianyu Zhang[63], Jiawei Zhang[1,63], L.M. Zhang[61], L.Q. Zhang[59], Lei Zhang[43], P. Zhang[1,63], Q.Y. Zhang[40,81], Shuihan Zhang[1,63], Shulei Zhang[26,h], X.D. Zhang[46], X.M. Zhang[1], X.Y. Zhang[50], Xuyan Zhang[55], Y. Zhang[69], Y. Zhang[72], Y. T. Zhang[81], Y.H. Zhang[1,58], Yan Zhang[71,58], Yao Zhang[1], Z.H. Zhang[1], Z.L. Zhang[35], Z.Y. Zhang[44], Z.Y. Zhang[76], G. Zhao[1], J. Zhao[40], J.Y. Zhao[1,63], J.Z. Zhao[1,58], Lei Zhao[71,58], Ling Zhao[1], M.G. Zhao[44], S.J. Zhao[81], Y.B. Zhao[1,58], Y.X. Zhao[32,63], Z.G. Zhao[71,58], A. Zhemchugov[37,a],

JHEP01(2024)180

B. Zheng[72], J.P. Zheng[1,58], W.J. Zheng[1,63], Y.H. Zheng[63], B. Zhong[42], X. Zhong[59], H. Zhou[50], L.P. Zhou[1,63], X. Zhou[76], X.K. Zhou[7], X.R. Zhou[71,58], X.Y. Zhou[40], Y.Z. Zhou[13,f], J. Zhu[44], K. Zhu[1], K.J. Zhu[1,58,63], L. Zhu[35], L.X. Zhu[63], S.H. Zhu[70], S.Q. Zhu[43], T.J. Zhu[13,f], W.J. Zhu[13,f], Y.C. Zhu[71,58], Z.A. Zhu[1,63], J.H. Zou[1], J. Zu[71,58]

[1] *Institute of High Energy Physics, Beijing 100049, People's Republic of China*
[2] *Beihang University, Beijing 100191, People's Republic of China*
[3] *Beijing Institute of Petrochemical Technology, Beijing 102617, People's Republic of China*
[4] *Bochum Ruhr-University, D-44780 Bochum, Germany*
[5] *Budker Institute of Nuclear Physics SB RAS (BINP), Novosibirsk 630090, Russia*
[6] *Carnegie Mellon University, Pittsburgh, Pennsylvania 15213, U.S.A.*
[7] *Central China Normal University, Wuhan 430079, People's Republic of China*
[8] *Central South University, Changsha 410083, People's Republic of China*
[9] *China Center of Advanced Science and Technology, Beijing 100190, People's Republic of China*
[10] *China University of Geosciences, Wuhan 430074, People's Republic of China*
[11] *Chung-Ang University, Seoul, 06974, Republic of Korea*
[12] *COMSATS University Islamabad, Lahore Campus, Defence Road, Off Raiwind Road, 54000 Lahore, Pakistan*
[13] *Fudan University, Shanghai 200433, People's Republic of China*
[14] *GSI Helmholtzcentre for Heavy Ion Research GmbH, D-64291 Darmstadt, Germany*
[15] *Guangxi Normal University, Guilin 541004, People's Republic of China*
[16] *Guangxi University, Nanning 530004, People's Republic of China*
[17] *Hangzhou Normal University, Hangzhou 310036, People's Republic of China*
[18] *Hebei University, Baoding 071002, People's Republic of China*
[19] *Helmholtz Institute Mainz, Staudinger Weg 18, D-55099 Mainz, Germany*
[20] *Henan Normal University, Xinxiang 453007, People's Republic of China*
[21] *Henan University, Kaifeng 475004, People's Republic of China*
[22] *Henan University of Science and Technology, Luoyang 471003, People's Republic of China*
[23] *Henan University of Technology, Zhengzhou 450001, People's Republic of China*
[24] *Huangshan College, Huangshan 245000, People's Republic of China*
[25] *Hunan Normal University, Changsha 410081, People's Republic of China*
[26] *Hunan University, Changsha 410082, People's Republic of China*
[27] *Indian Institute of Technology Madras, Chennai 600036, India*
[28] *Indiana University, Bloomington, Indiana 47405, U.S.A.*
[29] *INFN Laboratori Nazionali di Frascati , (A)INFN Laboratori Nazionali di Frascati, I-00044, Frascati, Italy; (B)INFN Sezione di Perugia, I-06100, Perugia, Italy; (C)University of Perugia, I-06100, Perugia, Italy*
[30] *INFN Sezione di Ferrara, (A)INFN Sezione di Ferrara, I-44122, Ferrara, Italy; (B)University of Ferrara, I-44122, Ferrara, Italy*
[31] *Inner Mongolia University, Hohhot 010021, People's Republic of China*
[32] *Institute of Modern Physics, Lanzhou 730000, People's Republic of China*
[33] *Institute of Physics and Technology, Peace Avenue 54B, Ulaanbaatar 13330, Mongolia*
[34] *Instituto de Alta Investigación, Universidad de Tarapacá, Casilla 7D, Arica 1000000, Chile*
[35] *Jilin University, Changchun 130012, People's Republic of China*
[36] *Johannes Gutenberg University of Mainz, Johann-Joachim-Becher-Weg 45, D-55099 Mainz, Germany*
[37] *Joint Institute for Nuclear Research, 141980 Dubna, Moscow region, Russia*
[38] *Justus-Liebig-Universitaet Giessen, II. Physikalisches Institut, Heinrich-Buff-Ring 16, D-35392 Giessen, Germany*
[39] *Lanzhou University, Lanzhou 730000, People's Republic of China*
[40] *Liaoning Normal University, Dalian 116029, People's Republic of China*
[41] *Liaoning University, Shenyang 110036, People's Republic of China*
[42] *Nanjing Normal University, Nanjing 210023, People's Republic of China*
[43] *Nanjing University, Nanjing 210093, People's Republic of China*

JHEP01(2024)180

[44] Nankai University, Tianjin 300071, People's Republic of China
[45] National Centre for Nuclear Research, Warsaw 02-093, Poland
[46] North China Electric Power University, Beijing 102206, People's Republic of China
[47] Peking University, Beijing 100871, People's Republic of China
[48] Qufu Normal University, Qufu 273165, People's Republic of China
[49] Shandong Normal University, Jinan 250014, People's Republic of China
[50] Shandong University, Jinan 250100, People's Republic of China
[51] Shanghai Jiao Tong University, Shanghai 200240, People's Republic of China
[52] Shanxi Normal University, Linfen 041004, People's Republic of China
[53] Shanxi University, Taiyuan 030006, People's Republic of China
[54] Sichuan University, Chengdu 610064, People's Republic of China
[55] Soochow University, Suzhou 215006, People's Republic of China
[56] South China Normal University, Guangzhou 510006, People's Republic of China
[57] Southeast University, Nanjing 211100, People's Republic of China
[58] State Key Laboratory of Particle Detection and Electronics, Beijing 100049, Hefei 230026, People's Republic of China
[59] Sun Yat-Sen University, Guangzhou 510275, People's Republic of China
[60] Suranaree University of Technology, University Avenue 111, Nakhon Ratchasima 30000, Thailand
[61] Tsinghua University, Beijing 100084, People's Republic of China
[62] Turkish Accelerator Center Particle Factory Group, (A)Istinye University, 34010, Istanbul, Turkey; (B)Near East University, Nicosia, North Cyprus, 99138, Mersin 10, Turkey
[63] University of Chinese Academy of Sciences, Beijing 100049, People's Republic of China
[64] University of Groningen, NL-9747 AA Groningen, The Netherlands
[65] University of Hawaii, Honolulu, Hawaii 96822, U.S.A.
[66] University of Jinan, Jinan 250022, People's Republic of China
[67] University of Manchester, Oxford Road, Manchester, M13 9PL, United Kingdom
[68] University of Muenster, Wilhelm-Klemm-Strasse 9, 48149 Muenster, Germany
[69] University of Oxford, Keble Road, Oxford OX13RH, United Kingdom
[70] University of Science and Technology Liaoning, Anshan 114051, People's Republic of China
[71] University of Science and Technology of China, Hefei 230026, People's Republic of China
[72] University of South China, Hengyang 421001, People's Republic of China
[73] University of the Punjab, Lahore-54590, Pakistan
[74] University of Turin and INFN, (A)University of Turin, I-10125, Turin, Italy; (B)University of Eastern Piedmont, I-15121, Alessandria, Italy; (C)INFN, I-10125, Turin, Italy
[75] Uppsala University, Box 516, SE-75120 Uppsala, Sweden
[76] Wuhan University, Wuhan 430072, People's Republic of China
[77] Xinyang Normal University, Xinyang 464000, People's Republic of China
[78] Yantai University, Yantai 264005, People's Republic of China
[79] Yunnan University, Kunming 650500, People's Republic of China
[80] Zhejiang University, Hangzhou 310027, People's Republic of China
[81] Zhengzhou University, Zhengzhou 450001, People's Republic of China

[a] Also at the Moscow Institute of Physics and Technology, Moscow 141700, Russia
[b] Also at the Novosibirsk State University, Novosibirsk, 630090, Russia
[c] Also at the NRC "Kurchatov Institute", PNPI, 188300, Gatchina, Russia
[d] Also at Goethe University Frankfurt, 60323 Frankfurt am Main, Germany
[e] Also at Key Laboratory for Particle Physics, Astrophysics and Cosmology, Ministry of Education; Shanghai Key Laboratory for Particle Physics and Cosmology; Institute of Nuclear and Particle Physics, Shanghai 200240, People's Republic of China
[f] Also at Key Laboratory of Nuclear Physics and Ion-beam Application (MOE) and Institute of Modern Physics, Fudan University, Shanghai 200443, People's Republic of China
[g] Also at State Key Laboratory of Nuclear Physics and Technology, Peking University, Beijing 100871, People's Republic of China
[h] Also at School of Physics and Electronics, Hunan University, Changsha 410082, China

JHEP01(2024)180

[i] *Also at Guangdong Provincial Key Laboratory of Nuclear Science, Institute of Quantum Matter, South China Normal University, Guangzhou 510006, China*
[j] *Also at Frontiers Science Center for Rare Isotopes, Lanzhou University, Lanzhou 730000, People's Republic of China*
[k] *Also at Lanzhou Center for Theoretical Physics, Lanzhou University, Lanzhou 730000, People's Republic of China*
[l] *Also at the Department of Mathematical Sciences, IBA, Karachi 75270, Pakistan*

JHEP01(2024)180